Article

Correlation between Isoniazid Resistance and Superoxide Reactivity in *Mycobacterium tuberculosis* KatG

Reza A. Ghiladi, Katalin F. Medzihradszky, Frank M. Rusnak, and Paul R. Ortiz de Montellano

J. Am. Chem. Soc., **2005**, 127 (38), 13428-13442• DOI: 10.1021/ja054366t • Publication Date (Web): 02 September 2005

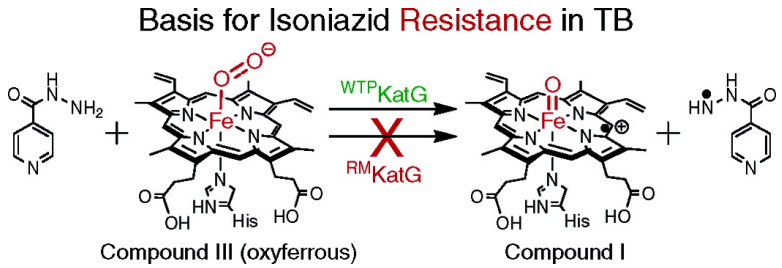

More About This Article

Additional resources and features associated with this article are available within the HTML version:

- Supporting Information
- Links to the 5 articles that cite this article, as of the time of this article download
- Access to high resolution figures
- Links to articles and content related to this article
- Copyright permission to reproduce figures and/or text from this article

View the Full Text HTML

J|A|C|S
ARTICLES
Published on Web 09/02/2005

Correlation between Isoniazid Resistance and Superoxide Reactivity in *Mycobacterium tuberculosis* KatG

Reza A. Ghiladi,[†] Katalin F. Medzihradszky,[†] Frank M. Rusnak,[‡] and Paul R. Ortiz de Montellano*[,†]

Contribution from the Department of Pharmaceutical Chemistry, University of California, San Francisco, California 94143-2280, and Department of Biochemistry and Molecular Biology and Section of Hematology Research, Mayo Clinic and Foundation, Rochester, Minnesota 55905

Received July 1, 2005; E-mail: ortiz@cgl.ucsf.edu

Abstract: Isoniazid is an antituberculosis prodrug that requires activation by the catalase-peroxidase (KatG) of *Mycobacterium tuberculosis*. The activated species, presumed to be an isonicotinoyl radical, couples to NADH forming an isoniazid−NADH adduct that ultimately confers antitubercular activity. We have compared the catalytic properties of three KatGs associated with isoniazid resistance (*r*esistance *m*utation KatGs, ^{RM}KatGs: R104L, H108Q, S315T) to wild-type enzyme and two additional lab mutations (*w*ild-*t*ype *p*henotype KatGs, ^{WTP}KatGs: WT KatG, Y229F, R418L). Neither catalase nor peroxidase activities, nor the presence/absence of the Met-Tyr-Trp cross-link (as probed by LC/MS on tryptic digests of the protein), exhibited any correlation with isoniazid resistance. The yields of isoniazid−NADH adduct formed were determined to be 1−5, 4−12, and 20−70-fold greater for the ^{WTP}KatGs than the ^{RM}KatGs for the compound I, II, and III pathways, respectively, strongly suggesting a role for oxyferrous KatG (supported by superoxide consumption measurements) that correlates with drug resistance. Stopped-flow UV−visible spectroscopic studies revealed that all KatGs were capable of forming both compound II and III intermediates. Rates of compound II decay were accelerated 4−12-fold in the presence of isoniazid (vs absence) for the ^{WTP}KatGs but were unaffected by the drug for the ^{RM}KatGs. A mechanism for isoniazid resistance which accounts for the observed reactivity for each of the compound I, II, and III intermediates is proposed and suggests that the compound III pathway may be the primary factor in determining overall isoniazid resistance by specific KatG mutants, with secondary contributions arising from the compound I and II pathways.

Introduction

Tuberculosis (TB) is one of the leading causes of death due to a single disease, claiming upward of 2 million lives each year.[1] With approximately one-third the world's population currently infected, it is estimated that between 2005 and 2020, nearly 1 billion people will be newly infected, over 125 million people will get sick, and 30 million will die of TB if control is not further strengthened. Despite the many successes achieved in the past 50 years using antibiotics to treat infectious diseases, the number of worldwide cases and deaths due to TB have remained steady.

The foremost first-line antibiotic used worldwide to treat TB is isoniazid (INH, Figure 1).[2] Despite numerous and intensive studies, our knowledge of the mechanism of action of INH is limited. Although the details are still being investigated, the consensus opinion is that a *Mycobacterium tuberculosis* (*Mtb*) catalase-peroxidase (KatG) oxidizes isoniazid, a prodrug,[3−6] to an isonicotinoyl radical, which then couples to NADH.[7−11] The resulting INH−NADH adduct is a potent inhibitor of InhA, an enoyl acyl-carrier-protein reductase involved in *Mtb* cell wall

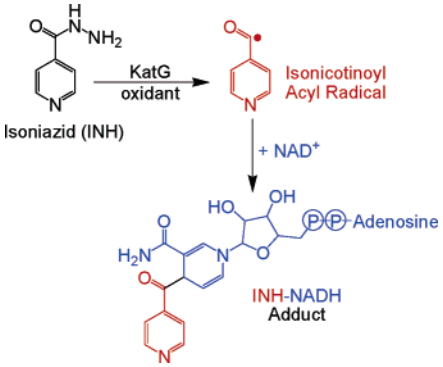

Figure 1. Schematic representation of INH−NADH adduct formation as catalyzed by KatG via an isonicotinoyl radical.

[†] University of California.
[‡] Mayo Clinic and Foundation.

(1) *Tuberculosis Fact Sheet, No 104*; World Health Organization: 2005.
(2) Zhang, Y. *Annu. Rev. Pharmacol. Toxicol.* **2005**, *45*, 529−564.
(3) Zhang, Y.; Heym, B.; Allen, B.; Young, D.; Cole, S. T. *Nature* **1992**, *358*, 591−593.
(4) Johnsson, K.; King, D. S.; Schultz, P. G. *J. Am. Chem. Soc.* **1995**, *117*, 5009−5010.
(5) Johnsson, K.; Schultz, P. G. *J. Am. Chem. Soc.* **1994**, *116*, 7425−7426.
(6) Scior, T.; Meneses Morales, I.; Garces Eisele, S. J.; Domeyer, D.; Laufer, S. *Arch. Pharm. Pharm. Med. Chem.* **2002**, *11*, 511−525.
(7) Rozwarski, D. A.; Grant, G. A.; Barton, D. H. R.; Jacobs, W. R., Jr.; Sacchettini, J. C. *Science* **1998**, *279*, 98−102.
(8) Lei, B.; Wei, C.-J.; Tu, S.-C. *J. Biol. Chem.* **2000**, *275*, 2520−2526.
(9) Nguyen, M.; Quemard, A.; Broussy, S.; Bernadou, J.; Meunier, B. *Antimicrob. Agents Chemother.* **2002**, *46*, 2137−2144.

10.1021/ja054366t CCC: $30.25

biosynthesis.[7,12] Inhibition of InhA by the INH−NADH adduct presumably results in a weakened mycobacterial cell wall and, ultimately, death of the pathogen. Similarly, it has been recently suggested that the antitubercular activity of isoniazid also arises from the coupling of INH$^{\bullet}$ to NADPH, forming an INH−NADPH adduct, which is an inhibitor of MabA, one of several proteins involved in the FAS-II mycolic acid synthesis pathway.[13] The origins of isoniazid drug-resistance in *Mtb* can be traced to point mutations in KatG that inhibit this "INH-oxidase" activity,[14−17] thereby raising the need to better understand the KatG mechanism and function.

Catalase-peroxidases (KatGs) are bifunctional hemoproteins belonging to Class I of the peroxidase superfamily (plants, fungi, and bacteria) and exhibit both catalatic ($H_2O_2 \rightarrow H_2O + {}^1/_2O_2$) and peroxidatic ($2AH + H_2O_2 \rightarrow 2A^{\bullet} + 2H_2O$) activities.[18] KatGs are anomalies: they have a high sequence homology with prokaryotic peroxidases, including fungal cytochrome *c* peroxidase and plant ascorbate peroxidase,[19] and as such possess substantial peroxidase activity, yet also exhibit catalatic activity equivalent to that of the monofunctional catalases despite having low sequence homology with the latter.[20] Additional enzymatic functions for KatGs have been described, including Mn^{2+}-dependent peroxidase,[21,22] cytochrome P450-like oxygenase,[23] and peroxynitritase activities.[24]

Interest in the catalase-peroxidases has also been spurred by the publication of three crystal structures of KatG from different sources: *Haloarcula marismortui*,[25] *Burkholderia pseudomonas*,[26] and *Mycobacterium tuberculosis*.[27] A common feature in each crystal structure is the presence of two covalent bonds between three amino acid side chains, Trp107, Tyr229, and Met255 (*Mtb* numbering) located on the distal side of the heme active site (Figure 2). The consistent observation of a Met-Tyr-Trp "cross-link" suggests that it is a characteristic common to all KatGs and, as it is not found in the monofunctional peroxidases, implies that this structural element may impart catalatic activity to the KatGs.[27] Indeed, several mutagenesis studies have confirmed that the cross-link is required for catalatic, but not peroxidatic, activity.[28−31]

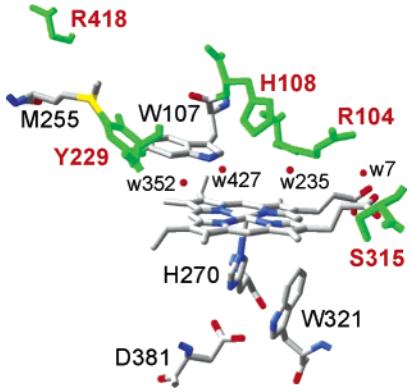

Figure 2. Heme environment of *Mtb* KatG. Active site residues (R418L, Y229F, R104L, H108Q, and S315T) which have been mutated in this work are displayed in green. Coordinates (1SJ2) were obtained from the Protein Data Bank.

Our previous work[32,33] has focused on elucidating the mechanism of INH oxidation by either wild-type KatG or KatG(S315T), a mutant that is found in greater than 50% of all clinical isolates harboring INH-resistance. The initial study[32] suggested that WT KatG, either as compound I [(Por$^{\bullet}$)Fe^{IV}=O, two-electron oxidized intermediate] or compound III [(Por)Fe^{III}−O_2^-, oxyferrous/ferric-superoxo adduct], was capable of oxidizing isoniazid. However, for KatG(S315T) only compound I was shown to oxidize INH, with oxyferrous KatG(S315T) being unable to do so. This correlation between superoxide reactivity and both INH oxidation in WT KatG (INH-susceptible) *and* lack of INH oxidation in KatG(S315T) (INH-resistant) led to the hypothesis that INH-resistance was due to the inability of oxyferrous KatG(S315T) to oxidize isoniazid.

We have shown[33] that the ability of oxyferrous KatG to oxidize INH in the presence of NADH, thereby forming the INH−NADH adduct, also correlates well with resistance, with WT KatG being able to carry out this reaction, and KatG(S315T) being unable to do so. Furthermore, UV−visible spectroscopic monitoring of oxyferrous KatG formed via pulse radiolysis suggested that oxyferrous WT KatG is reduced to compound II in the presence of INH, while under identical conditions oxyferrous KatG(S315T) remains unreacted.

While the previous work has established a direct correlation between oxyferrous KatG(S315T), suppressed levels of INH oxidation, and attenuated INH−NADH adduct formation (thereby leading to INH-resistance), a number of questions still remain. Is KatG(S315T) the only resistance mutation which exhibits this correlation? Do other mutations not associated with resistance show similar oxyferrous KatG reactivity patterns as WT KatG? Does the reaction between oxyferrous KatG and isoniazid consume superoxide, as our previously suggested mechanism

(10) Pierattelli, R.; Banci, L.; Eady, N. A. J.; Bodiguel, J.; Jones, J. N.; Moody, P. C.; Raven, E. L.; Jamart-Grégoire, B.; Brown, K. A. *J. Biol. Chem.* **2004**, *279*, 39000−39009.
(11) Wilming, M.; Johnsson, K. *Angew. Chem., Int. Ed.* **1999**, *38*, 2588−2590.
(12) Dessen, A.; Quémard, A.; Blanchard, J. S.; Jacobs, W. R., Jr.; Sacchettini, J. C. *Science* **1995**, *267*, 1638−1641.
(13) Ducasse-Cabanot, S.; Cohen-Gonsaud, M.; Marrakchi, H.; Nguyen, M.; Zerbib, D.; Bernadou, J.; Daffe, M.; Labesse, G.; Quemard, A. *Antimicrob. Agents Chemother.* **2004**, *48*, 242−249.
(14) Rouse, D. A.; DeVito, J. A.; Li, Z.; Byer, H.; Morris, S. L. *Mol. Microb.* **1996**, *22*, 583−592.
(15) Musser, J. M.; Kapur, V.; Williams, D. L.; Kreiswirth, B. N.; van Soolingen, D.; van Embden, J. D. A. *J. Infect. Dis.* **1996**, *173*, 196−202.
(16) Ramaswamy, S.; Musser, J. M. *Tuber. Lung Dis.* **1998**, *79*, 3−29.
(17) Wei, C.-J.; Lei, B.; Musser, J. M.; Tu, S.-C. *Antimicrob. Agents Chemother.* **2003**, *47*, 670−675.
(18) Welinder, K. G. *Curr. Opin. Struct. Biol.* **1992**, *2*, 388−393.
(19) Welinder, K. G. *Biochim. Biophys. Acta* **1991**, *1080*, 215−220.
(20) Zamocky, M.; Regelsberger, G.; Jakopitsch, C.; Obinger, C. *FEBS Lett.* **2001**, *492*, 177−182.
(21) Zabinski, R. F.; Blanchard, J. S. *J. Am. Chem. Soc.* **1997**, *119*, 2331−2332.
(22) Magliozzo, R. S.; Marcinkeviciene, J. A. *J. Biol. Chem.* **1997**, *272*, 8867−8870.
(23) Magliozzo, R. S.; Marcinkeviciene, J. A. *J. Am. Chem. Soc.* **1996**, *118*, 11303−11304.
(24) Wengenack, N. L.; Jensen, M. P.; Rusnak, F.; Stern, M. K. *Biochem. Biophys. Res. Commun.* **1999**, *256*, 485−487.
(25) Yamada, Y.; Fujiwara, T.; Sato, T.; Igarashi, N.; Tanaka, N. *Nat. Struct. Biol.* **2002**, *9*, 691−695.
(26) Carpena, X.; Loprasert, S.; Mongkolsuk, S.; Switala, J.; Loewen, P. C.; Fita, I. *J. Mol. Biol.* **2003**, *327*, 475−489.
(27) Bertrand, T.; Eady, N. A. J.; Jones, J. N.; Jesmin; Nagy, J. M.; Jamart-Grégoire, B.; Raven, E. L.; Brown, K. A. *J. Biol. Chem.* **2004**, *279*, 38991−38999.
(28) Santoni, E.; Jakopitsch, C.; Obinger, C.; Smulevich, G. *Biopolymers* **2004**, *74*, 46−50.
(29) Jakopitsch, C.; Ivancich, A.; Schmuckenschlager, F.; Wanasinghe, A.; Poltl, G.; Furtmuller, P. G.; Ruker, F.; Obinger, C. *J. Biol. Chem.* **2004**, *279*, 46082−46095.
(30) Jakopitsch, C.; Kolarich, D.; Petutschnig, G.; Furtmuller, P. G.; Obinger, C. *FEBS Lett* **2003**, *552*, 135−140.
(31) Jakopitsch, C.; Auer, M.; Ivancich, A.; Ruker, F.; Furtmuller, P. G.; Obinger, C. *J. Biol. Chem.* **2003**, *278*, 20185−20191.
(32) Wengenack, N. L.; Hoard, H. M.; Rusnak, F. *J. Am. Chem. Soc.* **1999**, *121*, 9748−9749.
(33) Ghiladi, R. A.; Cabelli, D. E.; Ortiz de Montellano, P. R. *J. Am. Chem. Soc.* **2004**, *126*, 4772−4773.

implies? Is compound II [(Por)Fe^{IV}=O or (KatG$^{\bullet}$)Fe^{III}, 1e^- oxidized above resting state] KatG involved in INH−NADH adduct formation? Does the presence of the Met-Tyr-Trp cross-link affect INH oxidation chemistry, and do mutations which are INH-resistant lack it?

To address these and additional questions, we have expanded the previous studies, which were limited to WT KatG and KatG(S315T), to include four additional mutations: KatG(R418L), KatG(Y229F), KatG(R104L), and KatG(H108Q) (Figure 2). The former two represent lab mutations and, along with wild-type enzyme, will be referred to as ^{WTP}KatGs (*w*ild-*t*ype *p*henotype). The latter two have been identified as resistance mutations in clinical isolates and, along with KatG(S315T), shall be referred to as ^{RM}KatGs (for *r*esistance-associated *m*utations). We have examined the yield of the INH−NADH adduct formed for all six of these KatGs using oxidizing conditions which employ either compounds I, II, or III as mimics for the in vivo oxidizing species responsible for INH activation. Additionally, we have measured for each KatG the kinetic parameters (k_{cat}, K_m) for both catalase and peroxidase activities, to determine if any correlation between these activities and resistance exists. We have also measured the rate of superoxide consumption by KatG in the presence of both INH and NADH and have shown that superoxide is indeed utilized by the enzyme when forming the INH−NADH adduct. To determine whether the Met-Tyr-Trp cross-link plays a role in conferring resistance to the ^{RM}KatGs, tryptic digests in combination with LC−MS were employed to confirm the presence and/or absence of the cross-link in all six KatGs. Finally, stopped-flow UV−visible spectroscopic methods were employed to provide supporting evidence for a proposed mechanism that correlates isoniazid resistance to differences in the reactivity of compounds I, II, and III between the ^{WTP}KatGs and the ^{RM}KatGs.

Experimental Procedures

Materials. Isoniazid (INH), *tert*-butylhydroperoxide, hydrogen peroxide, 2,2′-azino-bis(3-ethylbenzothiazoline-6-sulfonic acid) diammonium salt (ABTS), and cytochrome *c* were purchased from Sigma-Aldrich. Buffer salts and acetonitrile (HPLC grade) were purchased from Fisher Scientific. All other reagents and biochemicals, unless otherwise specified, were purchased at the highest grade available. INH was recrystallized from methanol prior to use. SOTS-1 was prepared as described in the literature.[34,35] 2-Methyl-1-phenyl-2-propyl hydroperoxide (MPPH) was synthesized according to the published procedure.[36,37]

Plasmid Preparation, Protein Expression, and Purification. Recombinant WT KatG, KatG(S315T), and KatG(Y229F) were overexpressed in *Escherichia coli* as previously described.[33,38] For KatG(R418L), KatG(R104L), and KatG(H108Q), mutagenesis, plasmid preparation, and DNA sequencing were performed per published protocol[38] using the following mutagenic primers: R104L, 5′-CACTACGGGCCGCTGTTTATC***CTG***ATGGCGTGGCACGCTGCC-3′, 3′-GATAAACAGCGGCCCGTAGTGGCCGTAGTC-5′; H108Q, 5′-CTGTTTATCCGGATGGCGTGG***CAG***GCTGCCGGCACCTACCGC-3′, 3′-CCACGCCATCCGGATAAACAGCGGCCC-5′; R418L, 5′-GCCTGGTACAAGCTGATCCAC***CTA***GACATGGGTCCCGTTGCG-3′, 3′-GTGGATCAGCTTGTACCAGGCCTTGGC-5′. KatG(R418L), KatG(R104L), and KatG(H108Q) were overexpressed and purified as previously described for WT KatG,[33] with only minor modifications which are provided in the Supporting Information.

Spectroscopic Studies. Optical spectra were recorded on a Hewlett-Packard 8452A diode array spectrophotometer equipped with a thermostated cell holder at 25 °C. Protoheme content was measured by the pyridine hemochrome assay using $\Delta\epsilon_{557}$ = 20.7 mM^{-1} cm^{-1} (reduced − oxidized) for iron protoporphyrin IX.[39,40]

Enzyme Assays. All measurements were performed in octiplet using a SpectraMax Plus384 UV−visible plate reader equipped with 96-well plates. Assays were carried out at 37 °C in 100 mM potassium phosphate buffer (pH 7.5) containing 5 μM EDTA (200 μL total volume). Catalase activity was measured spectrophotometrically by following the decrease over 60 s (linear least-squares fittings) of the H_2O_2 concentration (1.5, 5, 10, 15, 30, and 60 mM) at 240 nm (ϵ_{240} = 43.6 M^{-1} cm^{-1}).[41] Enzyme concentrations were as follows: WT KatG, 10 nM; KatG(S315T), 15 nM; KatG(R104L), KatG(H108Q), KatG(R418L), 2.1 μM; KatG(Y229F), 20 μM. Peroxidase activity was measured by following the increase (linear least-squares fittings) over 60 s in absorbance for 1.0 mM ABTS (ϵ_{405} = 36.8 mM^{-1} cm^{-1})[42] in the presence of either *tert*-butyl hydroperoxide or MPPH (0.25, 2.5, and 25 mM) as noted in Table 1. Enzyme concentrations were as follows: WT KatG, KatG(S315T), KatG(H108Q), 500 nM; KatG(Y229F), KatG(R104L), KatG(R418L), 100 nM. Kinetic parameters (K_m, V_{max}) were obtained from nonlinear regression (least-squares fitting) of Michaelis−Menton plots using the GraFit 4 kinetics software package available from Erithacus Software (http://www.erithacus.com/).

INH−NADH Adduct Formation. Assays were performed in triplicate except where noted in Table 1. The reaction sample (0.5 mL total volume) contained 100 mM KP_i (pH 7.5), 5 mM EDTA, 10 nM catalase (except for when H_2O_2 was exogenously added), 6 μM KatG, 2 mM INH, 240 μM NADH, and either no exogenous oxidant ("air"/control), 400 μM *t*-BuOOH, 400 μM H_2O_2, 400 μM MPPH, or 1 mM SOTS-1 (yielding 400 μM superoxide). Samples were incubated at 37 °C and analyzed at t = 0 (control) and 1 h using 100 μL injection volumes. HPLC analyses were performed on a Hewlett-Packard 1090 Series II Liquid Chromatograph employing a reversed-phase C_{18} column (Alltech, 10 μm particle size, 100 Å, 4.6 mm i.d. × 250 mm, Nucleosil) using a nonlinear gradient from 0 to 15% acetonitrile in 70 mM ammonium acetate solution (flowrate: 1 mL/min; detection 220−500 nm). INH−NADH adducts were identified by their UV−visible absorption spectrum and characteristic A_{260}/A_{326} ratio as described in the literature,[8,9] and yields were determined from integration of the corresponding peak area using ϵ_{260} = 27 mM^{-1} cm^{-1} and ϵ_{326} = 6.9 mM^{-1} cm^{-1}.[8,9]

Superoxide Consumption Measurements. The rates of superoxide production by SOTS-1 in the presence and absence of KatG were determined spectrophotometrically by following the reduction of ferricytochrome *c* to ferrous cytochrome *c* (ϵ_{550} = 21 mM^{-1} cm^{-1})[43] via a SpectraMax Plus384 UV−visible plate reader spectrophotometer equipped with 96-well plates. The sample mixture (200 μL) contained the following: 100 mM KP_i (pH 7.5), 5 mM EDTA, 2 mM SOTS-1, 2 mM INH, 1.2 mM NADH, 500 μM cytochrome *c*, and either with or without (control) 6 μM KatG. Slopes (linear least-squares fittings) were calculated over 60 s (linear). All samples were repeated four times, and data reported as a percentage of superoxide consumed by KatG: $(1 - (slope_{data}/slope_{control})) \times 100\%$.

(34) Konya, K. G.; Paul, T.; Lin, S.; Lusztyk, J.; Ingold, K. U. *J. Am. Chem. Soc.* **2000**, *122*, 7518−7527.
(35) Ingold, K. U.; Paul, T.; Young, M. J.; Doiron, L. *J. Am. Chem. Soc.* **1997**, *119*, 12364−12365.
(36) Foster, T. L.; Caradonna, J. P. *J. Am. Chem. Soc.* **2003**, *125*, 3678−3679.
(37) Hiatt, R. R.; Strachan, W. M. J. *J. Org. Chem.* **1963**, *28*, 1893−1894.
(38) Ghiladi, R. A.; Knudsen, G. M.; Medzihradszky, K. F.; Ortiz de Montellano, P. R. *J. Biol. Chem.* **2005**, *280*, 22651−22663.
(39) Falk, J. E. *Porphyrins and Metalloporphyrins: Their General, Physical, and Coordination Chemistry and Laboratory Methods*; Elsevier Publishing: New York, 1964; pp 181−188.
(40) Fuhrhop, J. H.; Smith, K. M. In *Porphyrins and Metalloporphyrins*; Smith, K. M., Ed.; Elsevier Publishing: New York, 1975; pp 804−807.
(41) Beers, R. F., Jr.; Sizer, I. W. *J. Biol. Chem.* **1952**, *195*, 133−140.
(42) Childs, R. E.; Bardsley, W. G. *Biochem. J.* **1975**, *145*, 93−103.
(43) Fridovich, I. In *Handbook of Methods for Oxygen Radical Research*; Greenwald, R. A., Ed.; CRC Press: Boca Raton, FL, 1985; pp 213−215.

Table 1. Comparison of Catalase, Peroxidase, and INH−NADH Adduct Formation Activities and Superoxide Consumption for WT KatG and the Five Mutants

	^{WTP}KatGs			^{RM}KatGs		
	WT	R418L	Y229F	R104L	H108Q	S315T
			Catalase Activity			
k_{cat}, s^{-1}	6000 ± 70	33 ± 4	0.1 ± 0.05	3.6 ± 0.2	1.5 ± 0.1	3950 ± 100
K_m, mM	2.5 ± 0.2	16.7 ± 4.4	39.8 ± 6.4	10.5 ± 2.1	26.5 ± 3.5	6.4 ± 0.5
k_{cat}/K_m, (M^{-1} s^{-1})	2 400 000 ± 28 000	1988 ± 210	2.5 ± 1.3	346 ± 22	58 ± 4	610 000 ± 15 000
			Peroxidase Activity			
k_{cat}, s^{-1}	0.062 ± 0.001 (0.047 ± 0.002)[a]	0.119 ± 0.002	0.843 ± 0.056	0.124 ± 0.002	0.029 ± 0.003	0.051 ± 0.003 (0.043 ± 0.001)[a]
K_m, mM	8.44 ± 0.45 (11.9 ± 0.6)[a]	11.05 ± 0.52	2.66 ± 0.66	4.48 ± 0.21	2.06 ± 0.64	8.88 ± 1.48 (12.2 ± 0.3)[a]
k_{cat}/K_m, (M^{-1} s^{-1})	7.3 ± 0.4 (3.9 ± 0.2)[a]	10.7 ± 0.5	316 ± 39	28 ± 2	14 ± 3	5.7 ± 1.0 (3.5 ± 0.1)[a]
			INH−NADH Adduct Formation[b]			
air	2.07 ± 0.19	1.68 ± 0.15	1.51 ± 0.11	n.d.*	1.47 ± 0.02	1.19 ± 0.11
t-BuOOH	45.88 ± 2.96	7.28 ± 0.26	16.33 ± 2.38	8.75 ± 0.65	8.19 ± 0.58	21.32 ± 0.78
H_2O_2	n.d.[c]	17.19 ± 0.45	18.51 ± 2.05	8.19 ± 0.39	6.37 ± 0.19	n.d.[c]
MPPH	13.61 ± 2.38	18.40 ± 0.41	6.11 ± 0.26	1.36 ± 0.04	1.25 ± 0.13	1.30 ± 0.11
SOTS-1	19.92 ± 2.28	18.81 ± 0.52	16.22 ± 0.93	0.95 ± 0.13	0.89 ± 0.26	0.28 ± 0.24
			Superoxide Consumption			
% consumed	46.4 ± 1.1	43.3 ± 1.2	33.2 ± 4.0	4.2 ± 2.8	1.3 ± 2.7	−2.5 ± 3.7
Met-Tyr-Trp Cross-link formed	yes	yes	no	no	Tyr-Trp	yes
			MIC for BCG Expressing KatGs[14]			
μg/mL	0.5	n/a	n/a	>500	>500	90

[a] Determined with MPPH *in lieu* of *t*-BuOOH. [b] μmol. [c] n.d. = not detected (2 runs); n/a = not available.

Stopped-Flow UV−visible Spectrophotometry. Experiments were performed on a Hi-Tech SF-61 DX2 double mixing stopped-flow system employing a diode array spectrophotometer and were carried out at 25 °C in 100 mM KP_i (pH 7.5) containing 5 μM EDTA. The initial (premixing) concentrations were as follows: KatG, 20 μM; MPPH, 20, 50, or 200 μM; PAA, 20, 50, or 200 μM; H_2O_2, 0.2, 2, 20, 50, or 250 mM. Data were collected (300 scans) over 0.6, 6, 60, and 600 s using the KinetAsyst software package (Hi-Tech) and analyzed using the Specfit Global Analysis System software package (Spectrum Software Associates) as first-order reactions. Data were fit from one to three exponential curves where applicable.

Tryptic Digests and HPLC Analysis. 250 μL of a 50 μM solution of KatG (~1 mg protein) in 100 mM KP_i (pH 7.5) were incubated with 5 μg (200:1 protein/protease ratio) of sequencing grade modified trypsin (Promega) for 3 h at 37 °C. Following proteolytic digestion, the peptide fragments were separated using HPLC [ProSphere (Alltech) C_{18}, 5μ, 100 Å; buffer A: H_2O + 0.1% trifluoroacetic acid (TFA); buffer B: MeCN + 0.1% TFA; 0.5 mL/min; UV−visible spectroscopic monitoring (diode array): 200−600 nm]. The following elution profile was used: 0−14 min, 0% B (isocratic); 14−15 min, 0−30% B (linear); 15−25 min, 30% B (isocratic); 25−36 min, 30−36% B (linear). Fractions (0.5 mL) were collected, concentrated (SpeedVac), and submitted for MS analysis.

Mass Spectrometry. LC/MS analyses of the appropriate manually collected tryptic fractions were performed using a nanoHPLC system, consisting of an Eksigent nanopump and a Spark autosampler (column: C-18, 75 μm × 150 mm; solvent A: 0.1% formic acid in H_2O; solvent B: 0.1% formic acid in acetonitrile; flow rate: ~300 nL/min; linear gradient: 5−50% B over 30 min), and a QSTAR Pulsar (Applied Biosystems) quadrupole-orthogonal-acceleration-time-of-flight hybrid tandem mass spectrometer served as detector.

Results

Site-Directed Mutagenesis, Overexpression and Purification of KatG. The plasmid encoding wild-type KatG with an N-terminal poly-His tag (pMRLB11) was obtained from Colorado State University under the TB Research Materials and Vaccine Testing Contract (NIH, NIAID NO1 AI-75320). PCR amplification of pMRLB11 using mutagenic primers (5′-overlapping ends) directly produced linear mutated plasmid DNA, which could then be recircularized. DNA sequencing of the entire *katG* gene confirmed the success of the site-directed mutagenesis and the absence of secondary mutations. Hemin (30 mg/L) was added to the culture medium (prior to induction with IPTG) to ensure stoichiometric incorporation of the heme cofactor during overexpression in *E.coli*.[44] The two-part purification strategy (affinity followed by size-exclusion chromatographies) resulted in purification levels >95% homogeneity. Wild-type and mutant KatGs were indistinguishable by SDS−PAGE gels (see Figure S1). Typical yields of isolated, purified KatG ranged from 40 to 80 mg/L, indicating that the mutations did not drastically alter overall protein expression levels.

UV−visible Spectroscopy of KatG. The electronic absorption spectra of the KatGs are overlayed in Figure 3, and relevant spectral features and analysis are presented in Table S1. The optical purity ratio (Reinheitzahl or R_z, defined as A_{Soret}/A_{280}) for the KatGs varied from 0.53 to 0.65. While this alone suggests incomplete heme incorporation and presence of apoenzyme for several of the mutants, most notably KatG(S315T) and KatG(H108Q), it is refuted by pyridine hemochrome assays which yielded 0.97−1.04 heme/monomer, indicating holoenzyme for each KatG. Thus, the variation in R_z values can be attributed to extinction coefficient variance for the heme prosthetic group, arising from either direct influence of the mutation on the electronic structure of the heme or indirect from structural changes in the active site which lead to changes in heme coordination number or populations of spin states (see below). The R_z values for WT KatG (0.63), KatG(Y229F) (0.59),

(44) Wengenack, N. L.; Uhl, J. R.; St Amand, A. L.; Tomlinson, A. J.; Benson, L. M.; Naylor, S.; Kline, B. C.; Cockerill, F. R., III; Rusnak, F. *J. Infect. Dis.* **1997**, *176*, 722−727.

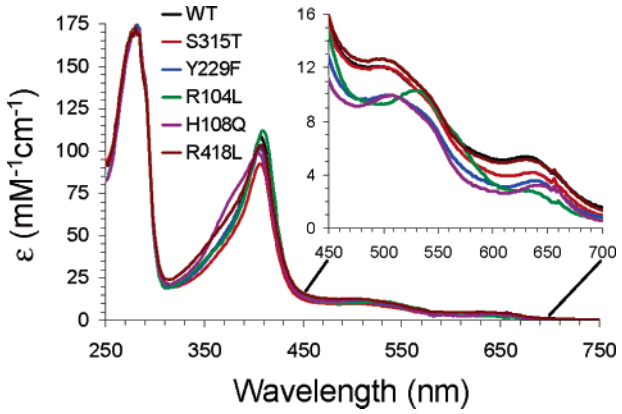

Figure 3. UV−visible absorption spectra of wild-type KatG and the five mutants KatG(R418L), KatG(Y229F), KatG(R104L), KatG(H108Q), and KatG(S315T) in 100 mM phosphate buffer (pH 7.5). Inset depicts the visible region in greater detail.

and KatG(S315T) (0.53) are each within the range reported for literature values.[38,45−48]

Although not the focus of the present study, as a detailed analysis by EPR and/or resonance Raman spectroscopies is required for sufficient quantitation, analysis of the electronic absorption spectrum can provide some basic insight into the coordination environment and spin-state of the heme present in KatG. As elegantly described by Magliozzo and co-workers,[49] analysis of the two ratios A_{Soret}/A_{380} and A_{614}/A_{645} is able to demonstrate relative populations of 6-coordinate (6-c) vs 5-c high spin (HS) heme. Generally, 5-c HS heme species exhibit a slightly blue shifted and smaller extinction Soret band than their 6-c HS counterparts, as well as a shoulder at 380 nm. Additionally, the CT1 feature in a 5-c HS heme is found at ∼640 nm (or higher), while that of a 6-c HS heme is generally closer to 630 nm. Furthermore, low spin (LS) heme systems exhibit a red-shifted Soret feature, the absence of a CT1 feature, and visible features at 565 and 580 nm. Thus, as can be seen from the data in Table S1, the relative amounts of 5-c HS heme in the four KatGs which lack a detectable (by optical spectroscopy) low-spin heme component are as follows: WT < S315T ≈ Y229F < H108Q. KatG(R104L) exhibits features consistent with the presence of a LS heme, notably 565 and 580 nm absorption bands, and a large red-shift in the β band. Additionally, the near absence of a CT1 band in KatG(R104L) suggests the presence of only a minor amount of HS heme in what is a predominantly LS system. KatG(R418L) appears to be an anomaly, as the position of the CT1 band as well as the A_{614}/A_{645} ratio is indicative of 6-c HS heme, but the presence of a shoulder at 380 nm and relatively low A_{Soret}/A_{380} suggest a five-coordinate heme. Further studies, including EPR spectroscopy, will hopefully shed better light on this aberration.

Catalase and Peroxidase Activities of KatG. Michaelis−Menton plots for catalase and peroxidase activities of the six purified KatGs are shown in Figure 4A and B, respectively,

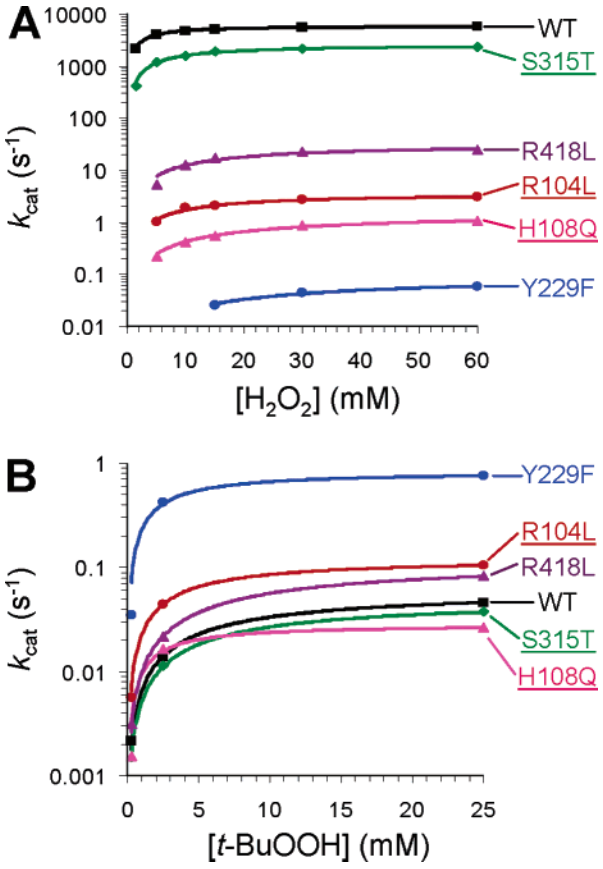

Figure 4. Michaelis−Menten plots for catalase (A) and peroxidase (B) activity measurements for the six KatGs. The ^{RM}KatGs are underlined, and nonlinear regression (least-squares fitting) is also shown.

and kinetic parameters derived therefrom are reported in Table 1. As catalases do not follow typical Michaelis−Menten kinetics (lack of a detectable enzyme−substrate complex and inability to reach saturation with H_2O_2 before inactivation), kinetic constants reported here for catalase activity are "apparent" values.[50,51] The KatGs, however, did exhibit saturable catalase activity under the conditions employed for this kinetic study. The values of k_{cat} determined for WT KatG (6000 s^{-1}) and KatG(S315T) (3950 s^{-1}) are consistent with previously reported values,[44,46] although the K_m for both enzymes determined here is lower by ∼2.5-fold when compared to literature values.[44] Catalase activities for KatG(Y229F),[38,47] KatG(R418L), KatG(R104L), and KatG(H108Q) exhibited k_{cat} ∼10^3 lower than WT KatG, suggesting that these mutations disrupt the hydrogen bonding network critical for catalase activity. K_m is increased 4−16-fold for these mutations when compared to WT KatG, indicating that substrate binding is also affected by the changes in the active site. Although most KatG active site mutations do severely affect catalase activity, comparison of the catalytic efficiencies (k_{cat}/K_m) for catalase activity to MICs for INH (of BCG strains expressing mutant KatGs;[14] Table 1) do not demonstrate any apparent correlation between catalase activity and isoniazid resistance between the ^{WTP}KatGs and the ^{RM}KatGs.

(45) Wengenack, N. L.; Lopes, H.; Kennedy, M. J.; Tavares, P.; Pereira, A. S.; Moura, I.; Moura, J. J.; Rusnak, F. *Biochemistry* **2000**, *39*, 11508−11513.
(46) Yu, S.; Girotto, S.; Lee, C.; Magliozzo, R. S. *J. Biol. Chem.* **2003**, *278*, 14769−14775.
(47) Yu, S.; Girotto, S.; Zhao, X.; Magliozzo, R. S. *J. Biol. Chem.* **2003**, *278*, 44121−44127.
(48) Chouchane, S.; Lippai, I.; Magliozzo, R. S. *Biochemistry* **2000**, *39*, 9975−9983.
(49) Chouchane, S.; Girotto, S.; Kapetanaki, S.; Schelvis, J. P.; Yu, S.; Magliozzo, R. S. *J. Biol. Chem.* **2003**, *278*, 8154−8162.
(50) Nicholls, P.; Fita, I.; Loewen, P. In *Advances in Inorganic Chemistry: Heme-Fe Proteins*; Sykes, A. G., Mauk, G., Eds.; Academic Press: 2001; Vol. 51, pp 51−106.
(51) Mate, M. J.; Murshudov, G.; Bravo, J.; Melik-Adamyan, W.; Loewen, P. C.; Fita, I. In *Handbook of Metalloproteins*; Messerschmidt, A., Huber, R., Poulos, T. L., Weighardt, K., Eds.; John Wiley & Sons: Chichester, 2001; Vol. 1, pp 486−502.

Peroxidase activities (saturable) were measured for the one-electron oxidation of 2,2′-azino-bis(3-ethylbenzothiazoline-6-sulfonate) (ABTS) to the corresponding radical cation $ABTS^{\bullet+}$ by KatG in the presence of *tert*-butylhydroperoxide. With the exception of KatG(Y229F) (0.843 s^{-1}), the k_{cat} values for KatG(R418L) (0.119 s^{-1}) and the ^{RM}KatGs [KatG(R104L) (0.124 s^{-1}), KatG(H108Q) (0.029 s^{-1}), and KatG(S315T) (0.051 s^{-1})] were all within 2-fold of that measured for WT KatG (0.062 s^{-1}) (Table 1), indicating that active site mutations not involving the covalent adduct do not generally alter peroxidase function. The increase in peroxidase activity for KatG(Y229F) has been noted previously by Magliozzo and co-workers,[47] who suggested that, upon loss of the covalent adduct, the increase in peroxidase activity (with concomitant loss of catalase function) is due to enhanced formation and/or increased stabilization of the compound II intermediate that plays a role in the peroxidase, but not catalase, cycle.[38,47] It is also noteworthy that the active site mutations generally lower the K_m value for ABTS, thereby driving up the catalytic efficiencies above that for WT KatG. However, as was the case for catalase activity, peroxidase function does not appear to correlate with INH resistance. Additionally, MPPH was substituted for *tert*-butylhydroperoxide in order to test the competency of this reagent in the peroxidase activity measurement. Both WT KatG (0.047) and KatG(S315T) (0.043) exhibited peroxidase activity that was only slightly attenuated when compared to the values determined for *t*-BuOOH, suggesting that the intermediate formed from the reaction between KatG and MPPH is capable of oxidizing ABTS (see Compound II Formation with MPPH below).

INH−NADH Adduct Formation. The amount of INH−NADH adduct (InhA-inhibitor) as catalyzed by both the ^{WTP}KatGs and the ^{RM}KatGs in the presence of various oxidants are reported in Table 1. Quantification of the INH−NADH adduct was performed by HPLC (Figure 5) using published protocols[9,52,53] with only slight modifications. Figure 5A depicts the HPLC chromatogram (A_{330}) for the formation of the INH−NADH adduct as catalyzed by WT KatG in the presence of air, *t*-BuOOH, and superoxide (delivered as SOTS-1) and is representative of the data tabulated in Table 1. The pattern of four peaks at t = 30.7, 31.2, 31.8, and 32.9 matches closely with that of the previously characterized four major isomers of the INH−NADH adduct[53] and exhibits the characteristic[8,9] UV−visible absorption spectrum (Figure 5B), with absorption maxima at 258 and 328 nm and $A_{258/328}$ = 3.2. Integration of the area under these four peaks, as well as the known extinction coefficient for the INH−NADH adduct, allowed for quantification of the yield of the adduct generated under various oxidizing conditions.

As a background control, the amount of INH−NADH adduct formed as catalyzed by KatG in the absence of an exogenously added oxidant (i.e, air-only) was measured. Overall, the yield of adduct produced by the mutant KatGs were at most 2-fold lower (1.19−1.47 μmol) than that found for WT KatG (2.07 μmol), with the notable exception of KatG(R104L) for which no INH−NADH adduct was detected (Table 1). Oxidation of

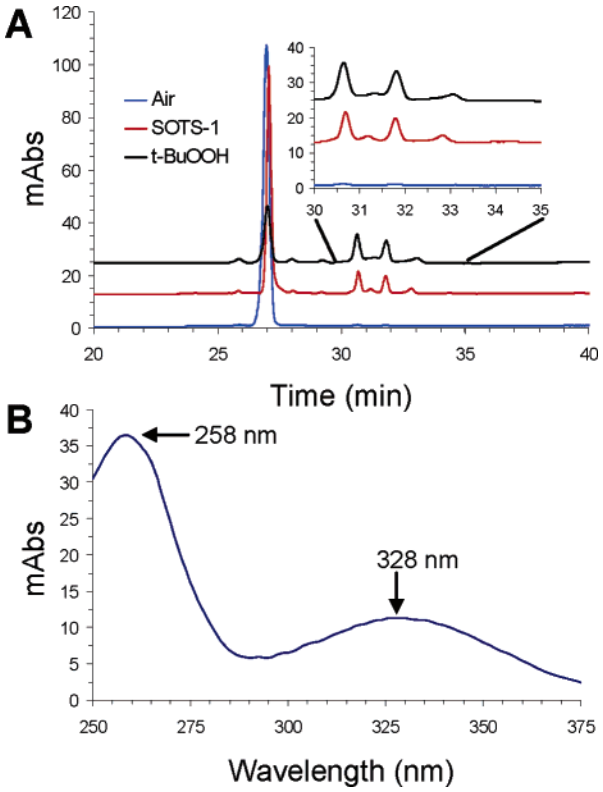

Figure 5. HPLC profiles (A, A_{330} chromatograms) depicting the formation of the INH−NADH adducts by WT KatG in the presence of air (blue), SOTS-1 (red), and *t*-BuOOH (black). The UV−visible spectrum of the INH−NADH adduct is also presented (B).

INH by KatG in the presence of air has been previously reported, with implications that such chemistry is mediated through an oxyferrous form of KatG. Several mechanisms exist for the spontaneous formation of oxyferrous KatG in solution, which has been previously shown to be a catalytically competent intermediate involved in the oxidation of INH: (i) trace N_2H_4 present in solutions containing INH was suggested to lead to KatG reduction, followed by dioxygen binding yielding an oxyferrous intermediate capable of oxidizing INH;[23,32] (ii) trace metals have been implicated in superoxide formation, either through oxidation of hydrazines in the presence of dioxygen or via trace-metal catalyzed autoxidation of INH at alkaline pH;[54−56] (iii) the NADH-oxidase activity of KatG (from *Burkholderia pseudomallei*) was also suggested to generate (in a pH-dependent reaction) either superoxide and/or hydrogen peroxide.[53] Generation of superoxide may lead to the catalytically competent oxyferrous KatG.[32,33] Hydrogen peroxide, generated either indirectly by the spontaneous disproportionation of superoxide in solution or directly by the NADH-oxidase activity, at low levels (i.e., substoichiometric concentrations which are not subject to the catalase activity of KatG) would presumably form compound I, an intermediate known to promote the formation of the INH−NADH adduct (see below). Overall, little difference was observed in the yields of the INH−NADH adduct between the ^{WTP}KatGs and the ^{RM}KatGs in the absence of any exogenously added oxidant.

(52) Nguyen, M.; Claparols, C.; Bernadou, J.; Meunier, B. *Chem. Biochem.* **2001**, *2*, 877−883.
(53) Singh, R.; Wiseman, B.; Deemagarn, T.; Donald, L. J.; Duckworth, H. W.; Carpena, X.; Fita, I.; Loewen, P. C. *J. Biol. Chem.* **2004**, *279*, 43098−43106.
(54) van der Walt, B. J.; van Zyl, J. M.; Kriegler, A. *Int. J. Biochem.* **1994**, *26*, 1081−1093.
(55) Hill, H. A.; Thornalley, P. J. *FEBS Lett.* **1981**, *125*, 235−238.
(56) Winder, F. G.; Denneny, J. M. *Biochem. J.* **1959**, *73*, 500−507.

Compound I catalyzed formation of the INH−NADH adduct was performed using *tert*-butylhydroperoxide, the same reagent used in the peroxidase activity measurements. For all KatGs, the presence of *t*-BuOOH in the reaction mixture increased the amount of the INH−NADH adduct produced by 5−20-fold over background, suggesting that compound I may play a significant and direct role in adduct formation. The yields observed for the ^{WTP}KatGs (7.28−45.88 μmol) were 1−5-fold higher than those observed for the ^{RM}KatGs (8.19−21.32 μmol). While this alone suggests a possible (albeit small) correlation to INH resistance, a few noteworthy comparisons are in order: (i) the difference in MIC between WT KatG and KatG(S315T) expressing BCG strains is 180×,[14] while the difference in the amount of INH−NADH adduct formed is only 2× (45.88 vs 21.32 μmol, respectively); (ii) the amount of adduct generated is 3× lower for KatG(Y229F) (16.33 μmol) and 6× lower for KatG(R418L) (7.28 μmol) than for WT KatG, yet no clinical isolates with these mutations have been identified to date; (iii) KatG(R104L) and KatG(H108Q) (8.75 and 8.19 μmol, respectively] generate 5−6× less adduct than WT KatG, but their MICs[14] are more than 10^3× higher. Given these comparisons, a correlation between the compound I pathway alone and isoniazid resistance is unlikely.

No adduct formation was detected for WT KatG and KatG(S315T) when H_2O_2 was utilized as an exogenous oxidant, presumably because of their high catalase activity. The absence of any detectable adduct was surprising, since we expected at least background (air-only) levels of the adduct present. We surmise that the hydrogen peroxide itself oxidizes any trace hydrazine in solution, thereby attenuating the air-only oxidation pathway. For KatG(Y229F), KatG(R104L), and KatG(H108Q), the amount of INH−NADH adduct observed for the H_2O_2-catalyzed reaction was comparable (within error) to that found for *t*-BuOOH, most likely due to the significantly impaired catalase function of these three KatGs. The one exception was KatG(R418L), which exhibited a 2-fold greater yield of the INH−NADH adduct for H_2O_2 when compared to *t*-BuOOH (17.19 vs 7.28 μmol) and most likely represents a greater binding affinity for hydrogen peroxide than *t*-BuOOH for this mutant.

Compound II catalyzed formation of the INH−NADH adduct was carried out using MPPH. For the ^{WTP}KatGs, the amount of adduct generated was increased 4−11-fold over the air-only controls (13.61, 18.40, and 6.11 μmol vs 2.07, 1.68, and 1.51 μmol, for WT KatG, KatG(R418L), and KatG(Y229F), respectively). These values are somewhat smaller than those determined for the compound I pathway yet are of significant magnitude to suggest that compound II is a competent oxidant for catalyzing INH−NADH adduct formation. In contrast, the amounts of adduct formed by the ^{RM}KatGs (1.36, 1.25, and 1.30 μmol for KatG(R104L), KatG(H108Q), and KatG(S315T), respectively) were found to be within error of the mean value for the corresponding background (air only) yield. Overall, the yield of the INH−NADH adduct was ∼10-fold *lower* for the ^{RM}KatGs than for WT KatG, suggesting a correlation between compound II reactivity and INH resistance.

Compound III catalyzed formation of the INH−NADH adduct was achieved by reacting resting enzyme with superoxide (delivered as SOTS-1). For the ^{WTP}KatGs, the amount of adduct formed was increased ∼10-fold over the air-only controls (19.92, 18.81, and 16.22 μmol vs 2.07, 1.68, and 1.51 μmol, for WT KatG, KatG(R418L), and KatG(Y229F), respectively]. These levels are on a par with those observed for both the compound I and II pathways, and such a significant yield enhancement suggests that compound III (oxyferrous) KatG is a catalytically competent species involved in INH−NADH adduct formation. In contrast, the amounts of adduct generated by the ^{RM}KatGs [0.95, 0.89, and 0.28 μmol for KatG(R104L), KatG(H108Q), and KatG(S315T), respectively] were found to be slightly *lower* than the mean value of the background level. More significantly, the ^{RM}KatGs exhibited INH−NADH adduct yields that were 20−70-fold lower than the ^{WTP}KatGs. These results show that mutations associated with resistance are strongly correlated with decreased yields of the INH−NADH adduct when superoxide is present, while wild-type enzyme and the two lab mutations have their adduct yields significantly elevated.

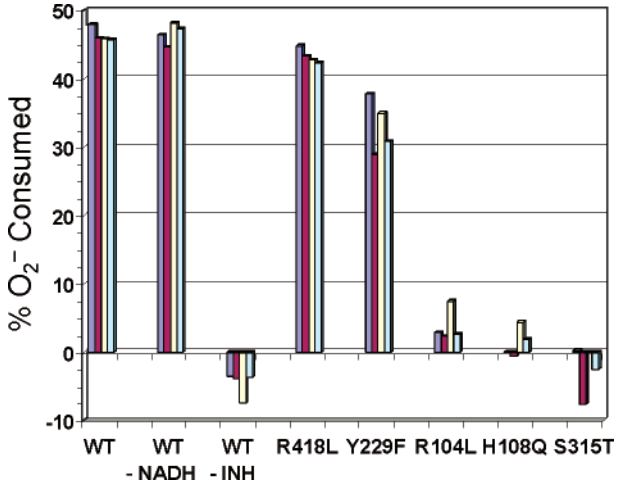

Figure 6. Percent of superoxide consumed by KatG (versus nonenzymatic control) during turnover forming the INH−NADH adduct as detected by the cytochrome *c* assay.

Superoxide Consumption Measurements. To confirm whether superoxide is a reagent for the KatG-catalyzed formation of the INH−NADH adduct, we have examined the rate of superoxide production by SOTS-1 (as detected by the classical cytochrome *c* assay) in a KatG-dependent manner. In the control experiment, the rate of superoxide production (i.e., capable of reducing cytochrome *c*) was measured in the presence of INH and NADH, but in the absence of KatG. The control rate was assigned a 100% value, with all other rates normalized to it. Upon addition of WT KatG to this solution, a 46.4 ± 1.1% reduction in the rate of superoxide production was found (Figure 6). This finding suggests that superoxide is consumed in the INH−NADH forming reaction, and is thus no longer available to reduce cytochrome *c* in the detection assay. Similarly, the other two ^{WTP}KatGs, KatG(R418L) and KatG(Y229F), also exhibited reduced rates of superoxide scavenging (43 and 33%, respectively), also suggesting that these two mutants consume superoxide in an enzyme-dependent reaction. Furthermore, the trend of superoxide consumption by these three KatGs, WT > R418L > Y229F, mirrors the trend observed for their rates of INH−NADH adduct formation when SOTS-1 is employed, again indicative of a strong correlation between superoxide consumption and INH−NADH adduct formation.

For the ^{RM}KatGs, their presence had a negligible effect on the amount of superoxide consumed (<4%) during the INH−NADH reaction. Indeed, this correlates well to the attenuated

Table 2. UV−visible Spectral Features and Kinetic Parameters for KatG Compound II

	λ_{max}	k_{obs} (M^{-1} s^{-1})	k_{-1} (s^{-1})	k_{-1}^{INH} (s^{-1})	ref
WT KatG	410, 628	$(4.8 \pm 0.4) \times 10^4$	0.095 ± 0.012	1.09 ± 0.12	*a*, 38
Synechocystis PCC 6803 KatG	407, 626[h]	n.d.	n.d.	n.d.	57
Anacystis nidulans KatG	406, ∼625[h]	n.d.	n.d.	n.d.	59
KatG(R418L)	408, 629	$(7.1 \pm 0.3) \times 10^3$	0.074 ± 0.010	0.94 ± 0.13	*a*
KatG(Y229F)	417, 531, 561	$(5.8 \pm 0.7) \times 10^6$	5.5 ± 0.3	19.7 ± 0.4	*a*, 38
KatG(Y229F)	416, 530, 560	*d*	*e*	*f*	47
Synechocystis PCC 6803 KatG(Y249F)	418, 530, 558	*g*	n.d.	n.d.	31
KatG(R104L)	bleach[b]	n.d.	0.213 ± 0.004[c]	0.222 ± 0.006[c]	*a*
KatG(H108Q)	bleach[b]	n.d.	0.122 ± 0.005[c]	0.114 ± 0.004[c]	*a*
KatG(S315T)	409, 628	$(2.3 \pm 0.2) \times 10^4$	0.031 ± 0.007	0.034 ± 0.009[c]	*a*

[a] This work. [b] Bleaching of the heme cofactor was observed with minor shifts in the absorption features which did not match any known intermediate spectrum. [c] Rate of heme bleach. [d] *Mtb* KatG(Y229F) reaction with PAA initially yielded compound I ($k_{obs} = \sim 4 \times 10^6$ M^{-1} s^{-1}), which underwent endogenous electron transfer to yield the oxoferryl compound II ($k_{obs} = (12.7-14.2) \pm 0.5$ s^{-1}). [e] Compound II was observed for ∼ 6 min when formed in the presence of PAA. [f] Conversion of compound II to resting enzyme was observed within 37.5 s after addition of INH. [g] *Synechocystis* PCC 6803 KatG(Y249F) reaction with PAA initially yielded compound I [$k_{obs} = (8.0 \pm 0.3) \times 10^6$ M^{-1} s^{-1}], which underwent endogenous electron transfer to yield the oxoferryl compound II ($k_{obs} = 0.6 \pm 0.1$ s^{-1}); n.d. = not determined. [h] Formed from the one-electron reduction of compound I (itself formed with PAA) with ascorbate.

rates of INH−NADH adduct produced by these three enzymes when superoxide is employed as the oxidant. The observation of superoxide consumption by the ^{WTP}KatGs versus a lack of superoxide consumption by the ^{RM}KatGs again supports a mechanism for INH−NADH adduct formation which is based upon superoxide reactivity and correlates well with INH resistance.

Similar rates for superoxide consumption by WT KatG were observed in both the presence and absence of NADH (46.4 ± 1.1 and 46.7 ± 1.5%, respectively), suggesting that NADH is not directly involved in the oxidation of INH by oxyferrous KatG. In the absence of INH, however, no superoxide consumption by WT KatG was observed (−4.7 ± 1.8%). In fact, the slight increase in the rate of superoxide production over that attributable to SOTS-1 alone suggests that WT KatG/NADH reactivity is capable of producing low levels of superoxide, a finding which has been previously noted for wild-type KatG from *Burkholderia pseudomallei*.[53]

Compound II Formation Using MPPH. As described previously for WT KatG and KatG(Y229F),[38] stopped-flow UV−visible spectroscopy was used to monitor the formation of the compound II intermediates of KatG(R418L) and KatG(S315T). Upon rapid mixing (2 ms) of a solution of ferric KatG (see Table S1 for spectral features) with MPPH, a new species was observed [UV−visible spectrum: ∼408−9 (Soret), ∼628−9 nm, Table 2] (Figures S2 and S3) whose spectral features matched neither those of KatG compound I [iron-oxo porphyrin π-cation radical; UV−visible spectrum (WT): 411 (Soret displays 40% hypochromicity vs resting), 550, 590, 655 nm][38,46,48] nor those of compound III [UV−visible: 413−8 (Soret), 539−45, 578−82 nm; Table 3]. The spectral features, however, were highly consistent (with respect to λ_{max} and extinction) with the previously characterized compound II intermediates of WT KatG,[38] *Synechocystis* PCC 6803 KatG,[57,58] and *Anacystis nidulans* KatG[59] (see Table 2 for spectral comparisons), with the latter two being observed in double-mixing stopped-flow experiments upon the 1 e^- reduction (ascorbate) of preformed KatG compound I. Based primarily on these UV−visible spectroscopic observations, as well as the fact that MPPH catalyzes the KatG-dependent oxidation of ABTS (vide infra, Table 1), we assign the new species detected here as the [(KatG$^{\bullet}$)(Por)]Fe^{III} compound II intermediates of *Mtb* KatG(R418L) and KatG(S315T). Values of k_{obs} for formation of this new species were linearly dependent on [MPPH] (2.5−10-fold excess per heme), giving bimolecular rate constants of $(7.1 \pm 0.3) \times 10^3$ M^{-1} s^{-1} for KatG(R418L) and $(2.3 \pm 0.2) \times 10^4$ M^{-1} s^{-1} for KatG(S315T). The intermediates were found to be unstable under these conditions, with a slow decay (0.074 and 0.031 s^{-1}, respectively) resulting in reformation of resting (ferric) enzyme, concomitant with a slight bleaching (∼5%) of the heme Soret band. Formation of a compound II intermediate from MPPH may occur by two different mechanisms. First, MPPH may serve both as the 2 e^- oxidant for resting KatG (heterolytic O−O bond cleavage) and as the one-electron substrate for the resulting compound I intermediate. This is analogous to the reactivity observed with *m*CPBA and either HRP[60] or KatG(Y229F),[47] where excess *m*CPBA served as a one-electron reductant for HRP compound I or KatG(Y229F) compound II, respectively. Alternatively, MPPH has been previously shown to undergo homolytic O−O bond

Table 3. UV−visible Spectral Features and Kinetic Parameters for KatG Compound III

	λ_{max}	k_{obs} (M^{-1} s^{-1})	ref
WT KatG	418, 545, 580	$>10^9$[b]	*c*
WT KatG[a]	415, 545, 580	$(4.47 \pm 0.91) \times 10^5$	33
WT KatG	418, 545, 580	n/a	48
Synechocystis PCC6803 WT KatG[b]	414, 548, 578	$(1.2 \pm 0.3) \times 10^5$[d]	63
KatG(R418L)	415, 542, 580	$>10^9$[b]	*c*
KatG(Y229F)	418, 545, 581	$(9.16 \pm 0.23) \times 10^5$	*c*
KatG(Y229F)	416, 543, 580	n/a	47
Synechocystis PCC6803 KatG(Y249F)[b]	414, 545, 578	$(1.6 \pm 0.2) \times 10^5$[d]	63
KatG(R104L)	413, 542, 579	$(1.75 \pm 0.11) \times 10^6$	*c*
KatG(H108Q)	413, 544, 582	$(8.54 \pm 0.17) \times 10^5$	*c*
KatG(S315T)	417, 539, 578	$>10^9$[b]	*c*
KatG(S315T)[a]	415, 545, 580	$(4.51 \pm 1.38) \times 10^5$	33

[a] Determined by pulse radiolysis (±3 nm resolution) for the reaction of ferric KatG with superoxide. [b] Formed within the mixing time (2 ms) of the stopped-flow instrument. [c] This work. [d] Formed by reaction of ferrous enzyme with dioxygen; n/a = not available.

(57) Regelsberger, G.; Jakopitsch, C.; Engleder, M.; Ruker, F.; Peschek, G. A.; Obinger, C. *Biochemistry* **1999**, *38*, 10480−10488.
(58) Regelsberger, G.; Jakopitsch, C.; Ruker, F.; Krois, D.; Peschek, G. A.; Obinger, C. *J. Biol. Chem.* **2000**, *275*, 22854−22861.
(59) Engleder, M.; Regelsberger, G.; Jakopitsch, C.; Furtmuller, P. G.; Ruker, F.; Peschek, G. A.; Obinger, C. *Biochimie.* **2000**, *82*, 211−219.
(60) Rodriguez-Lopez, J. N.; Hernandez-Ruiz, J.; Garcia-Canovas, F.; Thorneley, R. N.; Acosta, M.; Arnao, M. B. *J. Biol. Chem.* **1997**, *272*, 5469−5476.

cleavage in model complexes,[61] predominantly at pH values above 6.0,[62] resulting in compound II formation.

When similar conditions were employed to study the formation of compound II for KatG(R104L) and KatG(H108Q), only a rapid and irreversible bleaching of the heme was observed (data not shown). No intermediates matching compounds I, II, or III could be detected. This suggests that, in the absence of a one-electron reductant, formation of a compound II intermediate for these two KatGs may result in a loss of protein function due to modification of the heme cofactor.

Compound II was also observed during the reaction of KatG(Y229F) with H_2O_2 prior to formation of compound III, as has been previously noted by Magliozzo and co-workers.[47] Values of k_{obs} for formation of compound II were linearly dependent on [H_2O_2] (10−100 fold excess per heme), giving a bimolecular rate constant of $(2.8 \pm 0.3) \times 10^4$ M^{-1} s^{-1}. As noted above for this mutant, compound II was found to be unstable in the presence of excess hydrogen peroxide and quickly formed compound III.

Compound II Reduction by Isoniazid. Stopped-flow UV−visible spectroscopy was employed to monitor the reaction between KatG compound II and isoniazid. In a double mixing experiment, KatG (20 μM) was first mixed with a 10-fold excess of MPPH, allowed to incubate for 30 s, and then subsequently mixed with a 100-fold excess of INH. For WT KatG and KatG(R418L), a ∼12-fold acceleration in the rate of formation of resting (ferric) enzyme was observed in the presence of isoniazid, consistent with the notion that INH is a one-electron reducing agent for compound II (INH present: 1.1 and 0.94 s^{-1}; INH absent: 0.095 and 0.074 s^{-1}, respectively) (Table 2). KatG(Y229F) had a slightly lower 4-fold rate enhancement (19.7 vs 5.5 s^{-1}). Similar qualitative observations have been previously noted for the reaction of compounds I and/or II with isoniazid for WT KatG and KatG(Y229F).[47,48] For KatG(S315T), the rate of compound II to resting enzyme conversion was found to be nearly identical in the presence and absence of INH (0.031 vs 0.034 s^{-1}, Table 2), suggesting that INH is a poor reductant for this mutant. Due to the rapid bleaching of the heme cofactor for both KatG(R104L) and KatG(H108Q), a single mixing experiment in which KatG preincubated with INH was rapidly mixed with MPPH was performed in lieu of the double mixing protocol. Despite the presence of a large excess of isoniazid, bleaching of the heme was still observed on the same time scale as that previously seen in the absence of isoniazid. Overall, the compound II intermediates of the ^{WTP}KatGs were able to be reduced by INH, whereas those for the ^{RM}KatGs were unaffected by the presence of the drug, supporting the findings of the INH−NADH adduct formation study which suggested compound II may be implicated in an INH-resistance mechanism.

Compound II Oxidation by Peroxyacetic Acid (PAA). To determine if KatG compound II was capable of undergoing further oxidation, a double mixing stopped-flow experiment was performed in which compound II was first preformed as described above, followed by reaction with a 10-fold excess of peroxyacetic acid. For WT KatG, KatG(Y229F), KatG(R418L), and KatG(S315T), the compound II spectrum (see Table 2 for spectral features) was quickly converted to a new species [UV−visible spectrum: 408−412 (∼35−45% hypochromic Soret band), 545−50, 590−2, 645−55 (sh) nm], similar to those previously observed[38,48] for KatG compound I [UV−visible spectrum (WT): 411 (Soret displays 40% hypochromicity vs resting), 550, 590, 655 nm] (Figures S4−S7). Given that PAA is a two-electron oxidant, this implies the oxidation of compound II [(KatG$^{\bullet}$)Fe^{III}] to an intermediate one electron more oxidized than compound I, which we describe as [(KatG$^{\bullet}$)(Por$^{\bullet}$)-Fe^{IV}═O].

The double-mixing experiment was not performed for KatG(R104L) and KatG(H108Q) due to the inability to preform a stable compound II without bleaching of the heme cofactor.

Characterization of Compound III Intermediates by Optical Spectroscopy. Stopped-flow UV−visible spectroscopic methods were employed to detect the compound III intermediates of WT KatG and the five mutants (Figures S8−S13). Upon rapid mixing (2 ms) of a solution of ferric KatG [UV−visible spectral features are shown in Table S1] with H_2O_2 [250 mM for WT KatG, KatG(S315T); 0.2, 2, and 20 mM for KatG-(R418L), KatG(Y229F), KatG(R104L), and KatG(H108Q)], a new species was observed [UV−visible: 413−8 (Soret), 539−45, 578−82 nm; Table 3] whose absorption features matched neither those of KatG compound I [(Por$^{\bullet}$)Fe^{IV}═O; UV−visible spectrum: 411 (Soret displays 40% hypochromicity vs resting), 550, 590, 655 nm][38,46,48] nor those of compound II [(KatG$^{\bullet}$)Fe^{III} or (Por)Fe^{IV}═O; UV−visible spectrum: 410 (Soret), 628 nm, or ∼418 (Soret), ∼530, ∼560 nm, respectively].[31,38,47,57,59,63] The spectral features, however, were highly consistent (with respect to λ_{max} and extinction) with the previously characterized compound III intermediates of KatG from both *Mtb*[33,47,48] and *Synechocystis* PCC6803[63] (see Table 3).

WT KatG and KatG(S315T) possess significant catalase activity (k_{cat} = 3950−6000 s^{-1}; Table 1) such that reaction with H_2O_2 at low substrate concentrations (<1 mM) led to only minor changes in the optical spectrum (data not shown), inconsistent with compound III formation. At much higher [H_2O_2], the formation and decay of the oxyferrous intermediate could be observed, yet was hampered by excessive and disruptive oxygen evolution in the stopped-flow apparatus. Thus, it was only possible to observe compound III formation using a hydrogen peroxide concentration of 250 mM; higher concentrations of hydrogen peroxide led to far too much bubbling of O_2 in the sample chamber to obtain good quality spectra, while lower amounts of peroxide underwent disproportionation too rapidly to observe compound III formation. For both WT KatG and KatG(S315T), formation of compound III occurred within the mixing time of the stopped-flow apparatus (2 ms), corresponding to a bimolecular rate constant in excess of $\sim 10^9$ M^{-1} s^{-1} at 250 mM H_2O_2. This intermediate was found to be unstable at pH 7.5 and 25 °C, with a fast decay (0.3−0.4 s^{-1}) back to the resting ferric enzyme, presumably due to the high catalase activity of these two enzymes.

For KatG(R418L), formation of compound III also occurred within the mixing time of the stopped-flow apparatus (2 ms) for all concentrations of hydrogen peroxide examined, corresponding to a bimolecular rate constant in excess of $\sim 10^9$ M^{-1} s^{-1}. This intermediate was found to be unstable at pH 7.5 and 25 °C, with a slower decay (0.03 s^{-1}) back to the resting ferric

(61) Nam, W.; Han, H. J.; Oh, S.-Y.; Lee, Y. J.; Choi, M.-H.; Han, S.-Y.; Kim, C.; Woo, S. K.; Shin, W. *J. Am. Chem. Soc.* **2000**, *122*, 8677−8684.
(62) Nam, W.; Choi, H. J.; Han, H. J.; Cho, S. H.; Lee, H. J.; Han, S.-Y. *Chem. Commun.* **1999**, 387−388.
(63) Jakopitsch, C.; Wanasinghe, A.; Jantschko, W.; Furtmueller, P. G.; Obinger, C. *J. Biol. Chem.* **2005**.

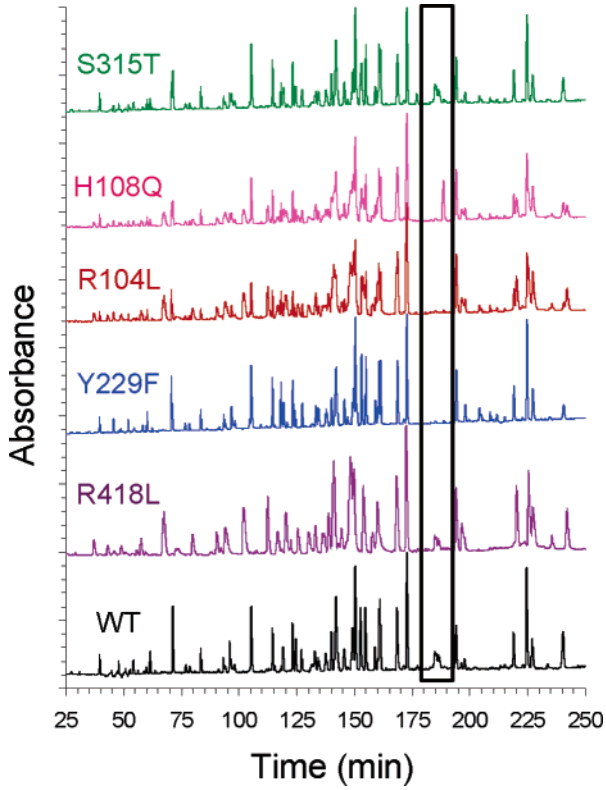

Figure 7. HPLC chromatograms (A_{220}) of the tryptic digests of KatG. The region ~185 min, denoting the time domain in which the Met-Tyr-Trp CLPF elutes, is highlighted.

enzyme than that observed for WT KatG or KatG(S315T). As KatG(R418L) does have a low level of catalase activity (k_{cat} = 33 s^{-1}; Table 1), this decay back to the resting enzyme could be due to a relatively slow enzyme-catalyzed disproportionation of hydrogen peroxide.

KatG(Y229F), KatG(R104L), and KatG(H108Q) are all extremely poor catalases (k_{cat} = 0.1−3.6 s^{-1}; Table 1) and, thus, are amenable to reaction with H_2O_2 at low concentrations in the stopped-flow apparatus. Values of k_{obs} for formation of compound III were linearly dependent on [H_2O_2] (10−100 fold excess per heme), giving bimolecular rate constants of ~10^5−10^6 M^{-1} s^{-1}. For KatG(Y229F), compound II formation was observable prior to compound III being detected (see below). Although the spectral features for these compound III intermediates were found to persist at pH 7.5 and 25 °C over the maximum observed time domain (60 s), presumably due to the lack of catalase activity and thus a lack of H_2O_2 disproportionation, a slow bleaching of the heme cofactor was nevertheless observed (~0.01−0.1 s^{-1}).

Identification of the Cross-Linked Peptide Fragments by Tryptic Digests of KatG. As we have previously reported for WT KatG (Met-Tyr-Trp cross-link present) and KatG(Y229F) (cross-link absent), the use of tryptic digestions of KatG in combination with high-pressure liquid chromatography and mass spectrometry has allowed identification of the peptide fragment containing the Met-Tyr-Trp cross-link (referred to as the *c*ross-*l*inked *p*eptide *f*ragment, CLPF).[38] Here, we have repeated this work with the remaining four KatGs, and HPLC chromatograms for all six are shown in Figure 7.

WT KatG, KatG(R418L), and KatG(S315T) all exhibit a peptide cluster at ~185 min, indicative of the CLPF. Additionally, they exhibit UV−visible spectral features at 254 and 300 nm that we have previously identified as being a spectroscopic signature that is unique to the Met-Tyr-Trp cross-link.[38] Mass spectrometry also identified the cross-linked component in each digest represented by ions at *m*/*z* 1147.7(6+), 983.9(7+), 861.0(8+), and 765.5(9+). The calculated monoisotopic neutral (zwitter ionic) mass of the CLPF is 6880.31 Da. No CLPF fragment was identified for either KatG(Y229F) or KatG(R104L). This was expected for KatG(Y229F), whose Tyr → Phe mutation would prevent such a cross-link from forming. To confirm the lack of a CLPF in KatG(R104L), additional digestions were performed with caspase, Asp-N, and proteinase K and compared to WT KatG digested under identical conditions (data not shown). In all cases, no peptide fragment possessing the UV−visible spectroscopic signature of the CLPF could be identified by HPLC. The lack of the Met-Tyr-Trp cross-link in KatG(R104L) may be due to the inability of the recombinant enzyme to form a stable compound I or compound II intermediate (see Discussion below) in the absence of the physiologically relevant substrate from *Mtb*, leading to rapid bleaching of the heme cofactor (vide supra). The presence of substrate has been previously shown in HRP to limit the extent of heme oxidation and protect the enzyme against inactivation by autoxidation.[64]

KatG(H108Q) also contained a CLPF, but its elution time (~190 min) was slightly shifted compared to that found for WT KatG. Initially, we believed this was due to the His → Gln mutation at position 108 which is contained within the [105−114] peptide of the CLPF. However, mass spectrometry, ions at *m*/*z* 1204.08(4+), and 963.47(5+), revealed that primarily only the Tyr-Trp cross-link was formed. (The calculated neutral monoisotopic mass is 4812.3 for the cross-linked ^{215}DLENPLAAVQMGLI**Y**VNPEGPNGNPDPM-AAAVDIR^{249} and ^{105}MA**W***Q*AAGTYR^{114} peptides.) The Met-Tyr-Trp containing CLPF was also detected, *m*/*z* 1146.2(6+), 982.6(7+), and 859.9(8+), for KatG(H108Q), although its intensity was significantly diminished when compared to the other KatGs. Furthermore, the UV−visible spectrum of the CLPF in KatG(H108Q) was found to be slightly shifted when compared to that of "pure" Met-Tyr-Trp CLPF from WT KatG (Figure S14). To better assess the relative ratio of Tyr-Trp:Met-Tyr-Trp, the UV−visible spectrum of the CLPF in KatG(H108Q) was modeled as a mixture between that observed for pure Tyr-Trp[65] and that seen for the Met-Tyr-Trp (from WT KatG). The spectral analysis suggests the CLPF contains >95+% Tyr-Trp cross-link, with the remainder represented by Met-Tyr-Trp. The lack of a fully formed Met-Tyr-Trp cross-link in KatG(H108Q) may be due to the similar inability to form a stable compound I/II intermediate as was found for KatG(R104L) (see Discussion below).

Discussion

Isoniazid resistance in *Mycobacterium tuberculosis* clinical isolates has been associated with either complete loss of the *katG* gene or a number of deletions, insertions, or point mutations within it. Of the roughly 40 mutations in the *katG*

(64) Colas, C.; Ortiz de Montellano, P. R. *Chem. Rev.* **2003**, *103*, 2305−2332.
(65) Ghiladi, R. A.; Medzihradszky, K. F.; Ortiz de Montellano, P. R. KatG(M255I) contains a methionine-to-isoleucine mutation and is, hence, unable to form the Met-Tyr-Trp cross-link. However, HPLC separation of tryptic digests in combination with LC−MS spectrometric characterization have identified a CLPF in KatG(M255I) as containing a Tyr-Trp cross-link. Manuscript in preparation.

gene which have been identified,[6,15,66] only a handful are located within the active site of the protein. The remainder appear to be located either on the surface of the protein, where they may play a role in governing KatG dimerization (KatG is a functional homodimer[27,67,68]), or in protein stability.[69] Disruption of hydrogen-bonding networks or electron-transfer pathways may also occur as a result of these mutations, but specific studies addressing these issues are still lacking. We have chosen to focus on the KatG mutations closest to the active site, as these would most likely relate to INH-activation processes governed by either the heme cofactor (i.e., oxidation by compounds I, II, or III) or the Met-Tyr-Trp cross-link.

Of the six KatGs examined in this study, three have been associated with INH resistance in clinical isolates: KatG(R104L), KatG(H108Q), and KatG(S315T) (^{RM}KatGs). The former two represent mutations in either the distal arginine or distal histidine residues, both of which have been shown to play essential roles in compound I/II formation and stabilization in the peroxidases.[70] The latter represents the most commonly occurring mutation associated with INH resistance in clinical isolates.[15,69,71] Of the remaining three KatGs, WT KatG, KatG(Y229F), and KatG(R418L) (^{WTP}KatGs), the latter two represent mutations which either wholly disrupt the formation of the Met-Tyr-Trp cross-link (Y229F), or could potentially disrupt the H-bonding networks within close proximity to it (R418L).

While it would be easy to surmise that the Met-Tyr-Trp cross-link would serve as a critical cofactor in INH activation, the presence or absence of the cross-link apparently does not appear to correlate with isoniazid resistance. Both WT KatG and KatG(S315T), the most commonly occurring mutation which confers INH resistance, were found to contain an intact Met-Tyr-Trp cross-link. Conversely, the lab mutation KatG(Y229F) and KatG(R104L), which has been associated with resistance, both lack the Met-Tyr-Trp cross-link. While the cross-link does not appear to be associated with INH resistance, it has a marked effect on the catalase activity of KatG: In the three mutants where the cross-link either has been completely eliminated (Y229F and R104L) or only partially formed (H108Q), catalase activity is essentially negligible ($k_{cat} \approx 0.1-3.6\ s^{-1}$) (Table 1). For the examples where the Met-Tyr-Trp cross-link is intact, catalase activity (k_{cat}) has a much broader range, from a low end of 33 s^{-1} (R418L) to 3950 and 6000 s^{-1} for KatG(S315T) and WT KatG, respectively. From a structural standpoint, Arg418 forms hydrogen bonds to several molecules of water which are in the vicinity of the Met-Tyr-Trp cross-link, and mutation of this residue may lead to disruption of the H-bonding network necessary for catalase activity. Thus, not only is an intact Met-Tyr-Trp cross-link required for catalase activity, but the H-bonding network responsible for delivering the protons necessary for catalatic activity must also be maintained. As the S315T mutation occurs >11 Å from the nearest contact of the Met-Tyr-Trp cross-link, the likelihood of a disrupted H-bonding network involved in catalase activity is low and is borne out by the fact that the k_{cat} value for this mutant is similar to that of wild-type enzyme.

By extension of the above trends, we can surmise that, for many of the KatGs that have been identified in the literature as lacking catalase activity and which at the same time possess insertions or deletions between residues Trp 107 and Tyr229, the attenuated catalase activity is most likely due to lack of formation of the Met-Tyr-Trp cross-link brought about by the incorrect spatial orientation of the three amino acids required for its formation. Thus, while these deletions and/or insertions may not significantly alter INH susceptibility or peroxidase activity (see below), they may prevent formation of the requisite cross-link for catalase activity.

For peroxidase activity, all mutants except KatG(Y229F) exhibited values for k_{cat} ($0.029-0.124\ s^{-1}$) that were within 2-fold of that for the wild-type enzyme ($0.062\ s^{-1}$) (Table 1). The rate acceleration for KatG(Y229F) ($0.843\ s^{-1}$) has been previously discussed[31,38,47] and is predicated on increased stabilization of the oxoferryl compound II intermediate. The kinetic data suggests that peroxidase activity is far less dependent upon the presence of the Met-Tyr-Trp adduct than catalase activity. This is not surprising, since KatGs share a high sequence homology with the peroxidases[18,19] (but not the catalases), implying that they inherently possess this activity independent of the cross-link.

Given that neither peroxidase nor catalase activities, nor the presence/absence of the Met-Tyr-Trp cross-link, are associated with the INH-resistance phenotype in the KatG mutations studied, we can now focus on our original supposition that INH−NADH adduct formation as catalyzed by the compound I/II/III intermediates of KatG may correlate with isoniazid susceptibility/resistance pathways in TB. For the compound I pathway, the amounts of INH−NADH adduct generated by the ^{RM}KatGs (8.19−21.32 μmol) were only marginally lower than those found for the ^{WTP}KatGs (7.28−45.88 μmol) and are in agreement with our previous observations that demonstrated a 2-fold difference in the rates of INH oxidation[32] and INH−NADH adduct formation[33] between WT KatG and KatG(S315T). Thus, this pathway cannot solely justify the 180−1000-fold difference in $MIC^{INH\ 14}$ between the ^{WTP}KatGs and the ^{RM}KatGs. The catalytic competence for INH oxidation by compound I for WT KatG[48] and the two resistance mutations KatG(S315T)[46] and KatG(W321F)[72] has been previously demonstrated by Magliozzo and co-workers, although these authors suggest that catalytic competence is also influenced by the higher k_d for INH in the mutant enzymes.

The amounts of INH−NADH adduct formed as catalyzed by compound II were found to be markedly different between the ^{WTP}KatGs (6.11−18.50 μmol) and the ^{RM}KatGs (1.25−1.36 μmol), mainly due to the fact that the WT-like KatGs exhibit a 4−12-fold increase in adduct production in the presence of MPPH, while the resistance mutation levels are comparable to those observed for the air-only controls. In support of these results, double-mixing stopped-flow UV−visible spectroscopy was used to directly monitor the reduction of preformed KatG compound II by isoniazid. For the ^{WTP}KatGs, the rate of decay of compound II and subsequent formation of the resting enzyme was accelerated 5−12-fold in the presence of INH relative to the rate in its absence (Table 2), suggesting that INH is a suitable

(66) Musser, J. M. *Clin. Microbiol. Rev.* **1995**, *8*, 496−514.
(67) Nagy, J. M.; Cass, A. E. G.; Brown, K. A. *J. Biol. Chem.* **1997**, *272*, 31265−31271.
(68) Johnsson, K.; Froland, W. A.; Schultz, P. G. *J. Biol. Chem.* **1997**, *272*, 2834−2840.
(69) Slayden, R. A.; Barry, C. E., III. *Microbes Infect.* **2000**, *2*, 659−669.
(70) Dunford, H. B. *Heme Peroxidases*; Wiley-VCH: New York, 1999.
(71) Heym, B.; Alzari, P. M.; Honoré, N.; Cole, S. T. *Mol. Microbiol.* **1995**, *15*, 235−245.
(72) Yu, S.; Chouchane, S.; Magliozzo, R. S. *Protein Sci* **2002**, *11*, 58−64.

one-electron reductant for compound II. A similar qualitative rate acceleration for KatG(Y229F) compound II reduction by INH has been previously noted by Magliozzo and co-workers.[47] For the ^{RM}KatGs, no such rate acceleration for compound II reduction by isoniazid was observed. The decay of KatG(S315T) compound II was unaffected by the presence of isoniazid (0.222 vs 0.213 s^{-1}), and while this intermediate could not be preformed for the R104L and H108Q mutants, the results from the single-mixing experiments with KatG and MPPH in the presence of INH gave similar values for the bleaching of the heme cofactor when compared to those observed in the absence of INH (Table 2).

The exact nature of compound II in KatG is still not clearly understood, as two distinct UV−visible spectra are associated with this intermediate (Table 2). One interesting possibility is that the spectral differences in compound II may be explained in light of two resonance structures for a 1 e^- oxidized state of KatG: (KatG)Fe^{IV}═O ⇆ (KatG$^•$)Fe^{III}—X (X = OH^- or H_2O), where KatG$^•$ represents a protein radical.[38,70,73,74] The former represents the "classical" oxoferryl species of the peroxidases (such as horseradish peroxidase) and is observed for KatG(Y229F) [UV−visible: ∼417 (Soret), ∼530, ∼560 nm],[31,38,47] whereas the latter represents the "catalase-peroxidase" compound II, occurring for all other KatGs [UV−visible: ∼408 (Soret), ∼625], and whose structure has been suggested to have an absorption spectrum only slightly perturbed from that of the resting enzyme.[57−59,70] As to the nature of the sixth axial ligand, we are unable to definitively assign it based on our spectroscopic evidence. Ferric-hydroxide complexes of HRP[75] and *Coperinus cinerius* peroxidase[76] are low spin (Q-band λ_{max} = 543, 575 nm), but several mutants of HRP[77] and C*c*P,[78] as well as wild-type myoglobin,[75] hemoglobin,[75] and FixL,[79] all exhibit thermal spin-state equilibria (HS/LS) for Fe^{III}—OH complexes (Q-band λ_{max} = ∼540, ∼580, ∼605 nm). Given that the compound II spectra of KatG all exhibit a minor feature at ∼545 nm as well as an absorption at ∼630 nm, a ferric-hydroxide LS/HS spin-state equilibrium is likely, but further studies are needed to provide support for this supposition.

As to the origin of the putative protein radical in (KatG$^•$)Fe^{III}, since KatG(Y229F) is the only mutant which exhibits the classical oxoferryl compound II spectrum (i.e., no protein-based radical),[38,47] we suggest that Tyr229 is responsible for initially reducing (KatG)Fe^{IV}═O to (KatG$^•$)Fe^{III}, concomitant with Tyr229$^•$ formation. The protein radical may migrate to other nearby redox active protein residues, as mutagenesis studies in conjunction with EPR spectroscopy on *Synechocystis* PCC 6803 KatG[80] have shown that Trp106 (Trp91 in *Mtb*) also forms a protein radical. Interestingly, Trp91 is part of an integral H-bonding network that includes Trp107 of the Met-Tyr-Trp cross-link, several active site waters, the heme propionate arm [to which KatG(S315T) is also hydrogen-bonded], and the catalytically important distal histidine (His108) and arginine (R104) residues. Given that the three ^{RM}KatGs all fall within this hydrogen-bonding network, the apparent inability for compound II to be reduced by isoniazid in these resistance mutations may arise from the mutation-induced disruption of this active site H-bonding network, or from differences in heme or side-chain redox potential, both of which could impact the proton-coupled/electron-transfer process required for protein-based radical reduction.

While the catalytic competence of compound II in INH activation has been shown by both the INH−NADH adduct formation studies and stopped-flow UV−visible spectroscopy, its relevance to INH-resistance pathways may be limited. Given that compound II is generally formed in vivo from compound I reduction, INH−NADH adduct formation should still occur via the compound I pathway prior to compound II being generated. Thus, while the compound II pathway does exhibit a sharp contrast in reactivity between the ^{WTP}KatGs and the ^{RM}KatGs in vitro, this observation may be a result of our ability to selectively generate compound II without the need to preform compound I.

In contrast to the observed compound I/II reactivity, compound III led to yields of the INH−NADH adduct that were 20−70-fold greater for the ^{WTP}KatGs than ^{RM}KatGs (16.22−19.92 μmol vs 0.28−0.95 μmol, respectively], supporting a role for superoxide which correlates well with INH resistance. Similar results were previously observed for the limited studies involving WT KatG and KatG(S315T)[32,38] and are in excellent agreement with the additional mutants examined here. In support of the role of superoxide in INH−NADH adduct formation, superoxide detection measurements (based on the classical cytochrome *c* method) were employed to determine the relative amount of free superoxide in solution in the presence and absence of KatG (Figure 6, Table 1). For the ^{WTP}KatGs, a marked reduction (33−46%) in the amount of superoxide present in solution was observed, suggesting that superoxide was being consumed by the INH−NADH adduct forming reaction in the presence of KatG. In contrast, little (if any) change in superoxide levels was observed for the ^{RM}KatGs (−2.5−4.2%), implying a lack of superoxide reactivity on their part. These results provide direct evidence that superoxide is playing an active role in the formation of the INH−NADH adduct.

To rule out a resistance mechanism based on the inability of a KatG mutant to form a compound III "oxyferrous" intermediate, we have generated this species for each KatG and characterized it using stopped-flow UV−visible spectroscopy. Four equivalent routes exist for generating compound III intermediates of KatG (or hemoproteins in general): (i) the reaction of the ferric enzyme with superoxide (by pulse radiolysis),[33] (ii) the reaction of the ferric enzyme with H_2O_2,[48] (iii) reaction of the ferrous enzyme with dioxygen,[63] or (iv) reacting the compound II intermediate with H_2O_2.[47,63] As benchtop sources of superoxide are unstable in aqueous solution and/or unsuitable for use in the stopped-flow apparatus, we have chosen the well-known reaction[70] between a ferric hemoprotein and excess hydrogen peroxide as the means to achieve KatG compound III formation. As expected, for WT KatG and

(73) Coulson, A. F. W.; Erman, J. E.; Yonetani, T. *J. Biol. Chem.* **1971**, *246*, 917−924.
(74) Ho, P. S.; Hoffman, B. M.; Solomon, N.; Kang, C. H.; Margoliash, E. *Biochemistry* **1984**, *23*, 4122−4128.
(75) Feis, A.; Marzocchi, M. P.; Paoli, M.; Smulevich, G. *Biochemistry* **1994**, *33*, 4577−4583.
(76) Smulevich, G.; Neri, F.; Marzocchi, M. P.; Welinder, K. G. *Biochemistry* **1996**, *35*, 10576−10585.
(77) Howes, B. D.; Rodriguez-Lopez, J. N.; Smith, A. T.; Smulevich, G. *Biochemistry* **1997**, *36*, 1532−1543.
(78) Smulevich, G.; Miller, M. A.; Kraut, J.; Spiro, T. G. *Biochemistry* **1991**, *30*, 9546−9558.
(79) Lukat-Rodgers, G. S.; Rexine, J. L.; Rodgers, K. R. *Biochemistry* **1998**, *37*, 13543−13552.
(80) Ivancich, A.; Jakopitsch, C.; Auer, M.; Un, S.; Obinger, C. *J. Am. Chem. Soc.* **2003**, *125*, 14093−14102.

Scheme 1. Proposed Mechanism for the Activation of Isoniazid by KatG

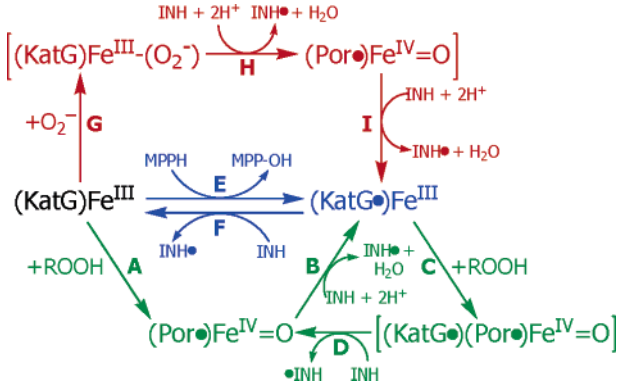

KatG(S315T), the compound III spectra [UV−visible: 417−8 (Soret), 539−45, 578−80 nm] (Table 3) generated by this reaction were identical (within resolution of the instruments) to those previously observed for these two enzymes by pulse radiolysis ($Fe^{III} + O_2^{-}$),[33] thus validating the assumption that compound III formation is independent from the means used to generate it (i.e., superoxide vs H_2O_2). Similarly, compound III spectra [UV−visible: 413−8 (Soret), 542−5, 579−82 nm] were also recorded for KatG(R418L), KatG(Y229F), KatG(R104L), and KatG(H108Q), but at much lower [H_2O_2] (0.2−20 mM) due to their vastly impaired catalase activity relative to WT KatG or KatG(S315T). Overall, it was possible to generate the compound III intermediate for each KatG examined in this study, and we have thus excluded lack of compound III formation as the basis for attenuated rates of INH−NADH adduct formation for the superoxide-dependent pathway.

Given the new data presented here pertaining to the reactivity of KatG compound II in generating the INH−NADH adduct, as well as the additional insights provided by the current stopped-flow and previous pulse radiolysis UV−visible studies, we propose an updated mechanism for INH activation by KatG compounds I, II, and III (Scheme 1). For the compound I pathway (green), commencement of the reaction cycle begins with reaction of resting enzyme [(KatG)Fe^{III}] with peroxide (step A), yielding compound I [(KatG)(Por•)Fe^{IV}=O]. Reduction of this intermediate with INH (step B) yields compound II [(KatG•)(Por)Fe^{III} for all KatGs except Y229F; (KatG)(Por)-Fe^{IV}=O for Y229F], concomitant with formation of an isonicotinoyl radical (for generation of the INH−NADH adduct). Compound II is then reduced by INH back to the resting state (step F), thus completing the cycle A → B → F → A, but only for the ^{WTP}KatGs. For the ^{RM}KatGs, compound II does not react with INH (see compound II pathway below). While this should lead to enzyme inactivation and attenuated rates of INH−NADH adduct formation due to the meta-stable nature of this intermediate, this is not what is observed (rates of adduct formation for the ^{RM}KatGs are nearly equivalent to those for the ^{WTP}KatGs). This apparent conundrum is resolved by invoking a hypervalent compound I [(KatG•)(Por•)Fe^{IV}=O], formed from the oxidation of ^{RM}KatG compound II [(KatG•)(Por)Fe^{III}] by excess peroxide (step C). Reduction of the hypervalent compound I with INH leads to formation of compound I (step D), thus creating a cycling (B → C → D → B) in which the ^{RM}KatGs are able to turnover INH without invoking a return to the resting state via compound II reduction. Thus, for either the ^{WTP}KatGs or the ^{RM}KatGs, compound-I-dependent reaction cycles are proposed which oxidize INH, ultimately leading to the formation of the INH−NADH adduct observed for all KatGs under these conditions.

Support for a hypervalent compound I intermediate via the oxidation of compound II comes from the double mixing stopped-flow experiment in which preformed compound II was allowed to react with peroxyacetic acid. The intermediate generated exhibited spectral features which matched those for KatG compound I. As PAA is an obligate two-electron oxidant, oxidation of compound II [(KatG•)(Por)Fe^{III}] would generate the hypervalent compound I species [(KatG•)(Por•)Fe^{IV}=O]. In (KatG•)Fe^{III}, the heme is essentially in the "resting" state and, therefore, capable of reacting with peracids or H_2O_2 to yield the hypervalent compound I intermediate. Thus, by transferring the oxidizing equivalent to a protein radical (Tyr229 or Trp91, for example), an oxoferryl intermediate can be avoided and activity is maintained. We have previously proposed a similar mechanism in which the catalase activity of KatG is maintained even in the compound II state, by invoking a hypervalent compound I species.[38]

The compound II pathway (Scheme 1, blue) begins with the one-electron oxidation of the resting enzyme [(KatG)Fe^{III}] with MPPH (step E), yielding compound II [(KatG•)(Por)Fe^{III} for all KatGs except Y229F; (KatG)(Por)Fe^{IV}=O for Y229F]. For the ^{WTP}KatGs, compound II is reduced by INH back to the resting state (step F), generating the isonicotinyl radical required for formation of the INH−NADH adduct. For the ^{RM}KatGs, compound II does not react with INH, no INH• is formed, and no INH−NADH adduct formation is observed. Thus, only for the ^{WTP}KatGs is a reaction cycle proposed (E → F → E) that is capable of generating the requisite isonicotinyl radical.

In the compound III pathway (Scheme 1, red), the cycle is initiated by reaction of superoxide with resting enzyme [(KatG)Fe^{III}], generating the oxyferrous compound III intermediate [(KatG)(Por)Fe^{III}−(O_2^{-})] (step G). As observed for WT KatG in our previous pulse radiolysis study, the presence of INH immediately generated the compound II spectrum, whereas under the same conditions KatG(S315T) remained unreacted (as compound III). The conversion of compound III to compound II in the presence of INH formally requires two additional electrons: the first 1e^{-} reduction would generate compound I (step H), while the second reducing equivalent would generate compound II (step I). These two individual steps were not observed in the pulse radiolysis experiments (implying a fast time scale electron transfer) but are inferred in this proposed mechanism based on the two-electron requirement for the observed compound III to compound II conversion. Thus, for the ^{WTP}KatGs, a cycle (G → [H → I] → E → G) initiated by superoxide binding to the resting enzyme and proceeding through compound I and II intermediates (due to reduction by the hydrazine moiety of INH and generation of INH•) is proposed. For the ^{RM}KatGs, no reaction or cycle is proposed that generates INH•, and hence no formation of the INH−NADH adduct is observed under these conditions.[81]

The in vitro studies presented here provide evidence that oxyferrous KatG is a critical intermediate involved in the activation of INH and that resistance to INH originates from mutations in KatG which disrupt this oxidation process, thereby inhibiting the formation of the INH−NADH adduct. In vivo evidence of superoxide involvement in the activation of INH

has also been reported. Burger and co-workers[82] have shown that *M. smegmatis* cultures transfected with *Mtb* KatG demonstrated increased susceptibility to INH (note: *M. smegmatis* is normally resistant to INH) upon addition of plumbagin, a superoxide generator. Moreover, superoxide dismutase effectively blocked the effect of added plumbagin, further implicating superoxide in the in vivo potentiation of INH toxicity. Furthermore, the addition of plumbagin and clofazamine, another O_2^- source, to *M. tuberculosis* H37Rv resulted in a 2−3-fold lowering of both the IC_{50} and the MIC for INH in the presence of these reagents, again suggesting a superoxide-dependent mechanism for INH activation.[83]

While the combination of the in vitro and in vivo studies strongly suggests that the reactivity of oxyferrous KatG with isoniazid represents the bifurcation between INH susceptible and resistant phenotypes, other factors contributing to isoniazid resistance in TB that do not involve superoxide must be considered. A decrease in binding affinity for INH by KatG(S315T) versus WT KatG (K_d = 400 μM vs 2.5 μM, respectively) has been noted by Magliozzo and co-workers[46] and has been suggested as a key factor in antibiotic resistance (MIC^{INH} = 90 vs 0.5 μg/mL, respectively; Table 1). On the other hand, KatG(W321G), which has also been identified as a resistance mutation (MIC^{INH} = >500 μg/mL), was found to have a K_d of 5.4 μM (measured for W321F), on a par with that of wild-type enzyme.[72] This suggests a lack of correlation between resistance and INH binding affinity. Additionally, KatG(Y229F) also exhibits a reduced binding affinity for INH (K_d = 133 μM)[47] on the order of that found for KatG(S315T), yet no clinical isolates associated with resistance have been found harboring this mutation. Thus, differences in binding affinity between WT KatG and certain KatG mutations, while perhaps contributing to the overall effect, are not the sole mitigating factor in determining absolute INH susceptibility or resistance. Furthermore, neither differences in superoxide-mediated active site reactivity nor isoniazid binding affinity are able to explain INH resistance due to mutations that are located at considerable distances from the active site or the substrate binding channel. These mutations may disrupt KatG dimerization (KatG is a functional homodimer[27,67,68]), reduce overall KatG stability,[69] or impede putative KatG/protein interactions which possibly occur in vivo.

As the three resistance mutations examined in this study are all found within the active site of KatG, several plausible explanations exist as to how the structural changes imparted by these mutations give rise to common functional changes, such as the inability of the ^{RM}KatGs to generate the INH−NADH adduct. Active site mutations have already been shown to affect the type of compound II intermediate observed in KatG [oxoferryl vs $(KatG^{\bullet})Fe^{III}$],[38] and this may play a role in the ability of this intermediate to oxidize INH. As noted earlier, an elaborate H-bonding network exists in the KatG active site that includes all three resistance mutations, the Met-Tyr-Trp cross-link, a heme propionate, several active site waters, as well as the redox active Trp91 residue. Thus, mutation of any one of these residues may lead to a common disruption of active site H-bonds which may be critical in regulating protein function or physical properties such as protonation events, heme or side-chain redox potential, or proton-coupled electron-transfer processes. Each one of these disruptions could, in turn, attenuate INH oxidation (by lowering the reduction potential of compounds I, II, or III, altering the pK_a of active site residues or waters, or promoting redox-active side-chain oxidation *in lieu* of INH oxidation, for example). Further studies are necessary to better understand if a single common mechanism exists in the three ^{RM}KatGs which confers an attenuated ability to oxidize INH.

Conclusions

The KatG from *M. tuberculosis* is responsible for the activation of isoniazid and formation of the INH−NADH adduct, the metabolite believed responsible for the antitubercular activity of isoniazid. Through comparisons between the ^{WTP}KatGs and ^{RM}KatGs, we have been able to show that neither of the two inherent KatG activities, catalase or peroxidase, correlate well to INH resistance. Furthermore, we have demonstrated that the presence of the Met-Tyr-Trp cross-link (or its absence) also does not correlate with drug resistance. However, when assaying for INH−NADH adduct formation, clear differences were observed. Foremost, superoxide reactivity via an oxyferrous KatG intermediate led to a 20−70-fold increase in the amount of INH−NADH adduct produced by the ^{WTP}KatGs when compared to the ^{RM}KatGs. A similar trend was also observed when a compound II pathway was invoked, but to a lesser extent (4−12-fold). The least differences (relative) in the amounts of INH−NADH adduct generated were found for the compound I pathway, where only a 1−5-fold increase in adduct production was observed for the ^{WTP}KatGs over the ^{RM}KatGs. Thus, it appears that the compound III pathway is most able to correlate with INH resistance, although contributions from the compound II pathway may also factor into a combined resistance profile. In support of an oxyferrous KatG-dependent pathway for INH−NADH adduct formation, cytochrome *c* assays confirmed the consumption of superoxide during KatG turnover when both INH and NADH were present.

The work presented in this study and previous pulse radiolysis and stopped-flow UV−visible spectroscopic measurements have been combined into a single proposed mechanism for INH activation by KatG which accounts for the differences in isoniazid susceptibility/resistance for the three pathways (compounds I, II, and III) examined here. Overall, while neither peroxidase nor catalase activities nor the presence or absence of the Met-Tyr-Trp cross-link correlates with the INH-resistance phenotype in KatG, critical comparisons of INH−NADH adduct formation apparently do and provide support for our original proposal that an oxyferrous/superoxide-dependent pathway may be crucial to understanding drug resistance in TB.

While much progress has been made on this front, many questions still persist. To what extent do each of the three pathways contribute to the overall resistance phenotype of a

(81) While it has been shown in this and other studies that INH is a suitable one-electron substrate for reducing compounds I and/or II, we cannot rule out the possibility that INH may act as a two-electron reductant in some steps, generating an acyldiimide, which upon loss of a diazene radical could generate $INH^{\bullet}$ (see Johnsson and Schultz, *J. Am. Chem. Soc.* **1994**, *116*, 7425−7426). Invoking INH as a two-electron reducing substrate in the proposed mechanism would combine H&I and B&F into single steps each. However, this would still yield the observed differences in INH−NADH adduct formation between the ^{WTP}KatGs and the ^{RM}KatGs for the reasons already outlined in the text.

(82) Wang, J.-Y.; Burger, R. M.; Drlica, K. *Antimicrob. Agents Chemother.* **1998**, *42*, 709−711.

(83) Bulatovic, V. M.; Wengenack, N. L.; Uhl, J. R.; Hall, L.; Roberts, G. D.; Cockerill, F. R., III; Rusnak, F. *Antimicrob. Agents Chemother.* **2002**, *46*, 2765−2771.

single KatG mutation? On which protein side chain does the radical reside in compound II [(KatG$^{\bullet}$)(Por)Fe^{III}], and do mutations which lead to resistance in the compound II pathway disrupt this radical formation? Is there a single structural basis for active site mutations which lead to isoniazid resistance (i.e., H-bonding network disruptions), or are multiple factors in play for each mutant? Studies addressing these and other important questions are in progress and will hopefully shed light on the mechanism of INH activation by KatG.

Acknowledgment. We thank Jessica D. Tenenbaum for discussions on hydrogen bonding to iron-oxo moieties. We also acknowledge the Colorado State University (NIH/NIAID Contract N01 AI-75320) for supplying the KatG-encoding plasmid pMRLB11. This work was supported by NIH Grant AI58524 (R.A.G. F32-Postdoctoral Fellowship), NCRR RR001614 and RR012961 (K.F.M., to the UCSF Mass Spectrometry Facility, director A.L. Burlingame), and GM56531 and GM32488 (P.O.M.).

Supporting Information Available: Full details of the overexpression and purification protocols of KatG. SDS-PAGE gel of all six KatGs (Figure S1). UV−visible spectroscopic data and analysis for the six KatGs (Table S1). Stopped-flow UV−visible spectra and analysis of the reaction of MPPH with KatG(R418L) (Figure S2) or KatG(S315T) (Figure S3). Double-mixing stopped-flow UV−visible spectra of the reaction between preformed compound II and peroxyacetic acid for WT KatG (Figure S4), KatG(R418L) (Figure S5), KatG(Y229F) (Figure S6), and KatG(S315T) (Figure S7). Stopped-flow UV−visible spectra and analysis for the reaction between H_2O_2 and WT KatG (Figure S8), KatG(R418L) (Figure S9), KatG(Y229F) (Figure S10), KatG(R104L) (Figure S11), KatG(H108Q) (Figure S12), and KatG(S315T) (Figure S13). UV−visible spectra of the cross-linked peptide fragments (CLPF) of WT KatG and KatG(H108Q) (Figure S14). This material is available free of charge via the Internet at http://pubs.acs.org.

JA054366T